

## Article

# Interaction of O<sub>2</sub> with Reduced Ceria Nanoparticles at 100–400 K: Fast Oxidation of Ce<sup>3+</sup> Ions and Dissolved H<sub>2</sub>

Kristina Chakarova , Nikola Drenchev , Mihail Mihaylov  and Konstantin Hadjiivanov \* 

Institute of General and Inorganic Chemistry, Bulgarian Academy of Sciences, 1113 Sofia, Bulgaria; ndrenchev@svr.igic.bas.bg (N.D.); misho@svr.igic.bas.bg (M.M.)

\* Correspondence: kih@svr.igic.bas.bg

**Abstract:** The interaction between O<sub>2</sub> and reduced ceria nanocubes was mainly investigated using FTIR spectroscopy. Nanorods and nanoparticles were also studied for comparison. Adsorption of O<sub>2</sub> at 100 K on unreduced ceria produces only O<sub>2</sub> molecularly adsorbed on Ce<sup>4+</sup> sites. The Ce<sup>3+</sup> cations on ceria reduced by H<sub>2</sub> at 773 K were monitored using the <sup>2</sup>F<sub>5/2</sub> → <sup>2</sup>F<sub>7/2</sub> electronic transition band at 2133–2095 cm<sup>-1</sup>. This band possesses a fine structure well resolved at 100 K. The positions of the individual components depend on the Ce<sup>3+</sup> environment, including the presence of nearby species such as OH groups. Even at 100 K, adsorption of O<sub>2</sub> on reduced ceria leads to fast oxidation of about half of the Ce<sup>3+</sup> cations, including all Ce<sup>3+</sup> sites bound to OH groups and carbonates, and the simultaneous formation of superoxo (O<sub>2</sub><sup>-</sup>) and peroxy (O<sub>2</sub><sup>2-</sup>) species. The remaining Ce<sup>3+</sup> sites disappear upon heating up to 348 K. At higher temperatures, the peroxy species decompose directly, yielding lattice oxygen. Superoxides are converted to hydroperoxides, which then decompose into terminal OH groups. Reduced samples evacuated at T < 773 K contain sorbed H<sub>2</sub>. Part of this hydrogen is also fast oxidized even at 100 K.

**Keywords:** ceria; oxidation; oxygen; nitrogen monoxide; nitrous oxide; FTIR spectroscopy



**Citation:** Chakarova, K.; Drenchev, N.; Mihaylov, M.; Hadjiivanov, K.

Interaction of O<sub>2</sub> with Reduced Ceria Nanoparticles at 100–400 K: Fast Oxidation of Ce<sup>3+</sup> Ions and Dissolved H<sub>2</sub>. *Catalysts* **2024**, *14*, 45. <https://doi.org/10.3390/catal14010045>

Academic Editor:  
Soghomon Boghosian

Received: 26 November 2023

Revised: 30 December 2023

Accepted: 7 January 2024

Published: 9 January 2024



**Copyright:** © 2024 by the authors. Licensee MDPI, Basel, Switzerland. This article is an open access article distributed under the terms and conditions of the Creative Commons Attribution (CC BY) license (<https://creativecommons.org/licenses/by/4.0/>).

## 1. Introduction

Ceria has found important industrial applications for various purposes, in particular, as a catalyst, catalyst component, support, or additive [1]. It is generally recognized that one of the key advantages of ceria in catalysis is its redox chemistry: under operating conditions, Ce<sup>4+</sup> cations on the surface can be easily and reversibly reduced to Ce<sup>3+</sup>, thereby forming oxygen vacancies, all without changing the crystallographic structure [2–4]. Thus, ceria can store and provide oxygen in the course of redox catalytic reactions. For the design of new efficient catalysts, detailed knowledge of the mechanism of oxidation and reduction of the ceria surface is extremely important. This knowledge is also essential for the biomedical applications of ceria nanoparticles [5,6].

Stoichiometric cerium dioxide is quite stable in the absence of reducing agents. For instance, TPD experiments show no substantial desorption of O<sub>2</sub> from the (111) ceria plane below 1300 K [7]. Exposure of ceria to reducing agents or energetic irradiation, however, can produce Ce<sup>3+</sup> sites on the surface even at much lower temperatures [4].

Many TPR studies have revealed that the reduction of ceria with hydrogen occurs in two steps [8–14]. During the first step, Ce<sup>4+</sup> cations situated on the surface are reduced, and this is reflected by one or more TPR peaks in the temperature range 685–835 K. Indeed, the ceria surface oxygen is mobile and can be easily removed at low temperatures [11,15]. Several research groups have reported a correlation between CeO<sub>2</sub> surface area and low-temperature hydrogen consumption [8,9,11,12]. Reduction of bulk takes place at higher temperatures (TPR peaks between 1010 and 1170 K) because of the low mobility of bulk oxygen and its difficult transport to the surface [11].

Although the general picture of ceria reduction by H<sub>2</sub> is clear, there are many factors affecting the precise interpretation of the TPR results. Different crystal faces are exposed on

the surface, and they are expected to have different reducibility. The presence of surface impurities, such as adsorbed oxygen, residual carbonates, etc. [9,12,16], may also provoke some variations in the TPR signal. Hydrogen adsorption and drop in surface area could also affect the low-temperature part of the TPR profile [12,16]. All this leads to a complex structure of the low-temperature TPR peak.

During the last two decades, many investigations have appeared on ceria nanoparticles with different well-defined shapes, e.g., nanocubes, nanorods, nanopolyhedra, etc. [5,6,17–21]. Each shape is characterized by a preferential exposure of one or more crystal facets on the surface. Although there is still disagreement in some details, these studies, in principle, allow for the estimation of the reactivity of one or another plane in a particular process.

A powerful technique for surface characterization is vibrational spectroscopy, mainly in its IR and Raman modes. It gives information on the surface hydroxyl coverage and the presence of some impurities, such as residual carbonates or nitrates. Moreover, this technique is unique for the determination of the structure of adsorbed species. Other important information, e.g., on the surface acidity, can be obtained using the so-called probe molecules. Especially for ceria, vibrational spectroscopy can also be used to follow its reduction degree. This is because the  $\text{Ce}^{3+} \ ^2\text{F}_{5/2} \rightarrow \ ^2\text{F}_{7/2}$  spin-orbit electronic transition is observed in the IR spectra as a separate band around  $2147\text{--}2110 \text{ cm}^{-1}$  [20,22–29]. Although the spectral region is wide, no attempts have been made to correlate the band position with  $\text{Ce}^{3+}$  sites in different environments.

While the reduction of ceria is relatively well studied, there are fewer works considering its reoxidation. Ayastuy et al. [14] studied temperature-programmed oxidation (TPO) of ceria just after a TPR run and observed one peak at 326 K, attributed to surface oxidation. Fally et al. [13] also found that oxidation of ceria pre-reduced at 973 K occurs easily, and the process is nearly completed even at 298 K. Similar results were reported for ceria reduced at 773 K [27]. It was also noted [30] that reduced ceria surfaces are not stable at ambient conditions and exhibit very fast reoxidation kinetic.

When ceria is reduced at high temperatures, and bulk reduction has occurred, the reoxidation occurs in steps below and above 473 K [31]. Therefore, it appears that just as bulk  $\text{Ce}^{4+}$  is more difficult to reduce than surface  $\text{Ce}^{4+}$ , oxidation of  $\text{Ce}^{3+}$  in the bulk is more difficult than on the surface.

IR Spectroscopic studies have revealed that  $\text{O}_2$  adsorption on reduced ceria leads to the formation of superoxide ( $\text{O}_2^-$ ) [32–34] and peroxide ( $\text{O}_2^{2-}$ ) species [33,34]. Similar results have been obtained using Raman spectroscopy [17,19,35]. Superoxide is characterized by a  $\nu(\text{O-O})$  band at  $1139\text{--}1127 \text{ cm}^{-1}$  and is stable up to 348 K [19]. Peroxide species are different kinds, and  $\nu(\text{O-O})$  was detected in the  $890\text{--}830 \text{ cm}^{-1}$  region [19,33]. They are more stable and disappear from the spectra after treatment above 473 K. A stepwise conversion between  $\text{O}_2$ ,  $\text{O}_2^-$ ,  $\text{O}_2^{2-}$ ,  $\text{O}^-$ , and lattice  $\text{O}^{2-}$  has been proposed [19,33]. Note that the production of superoxide and peroxide species leads to immediate (fast) oxidation of  $\text{Ce}^{3+}$ . This means that the redox process occurs simultaneously with adsorption.

In light of the above considerations, many studies reporting a significant concentration of  $\text{Ce}^{3+}$  ions on ceria samples pre-exposed to air seem surprising. Analysis of these results shows that, in most cases, the conclusions were made on the basis of results from two techniques: XPS and Raman spectroscopy.

An elegant proof of the reduction of ceria during XPS analysis was recently provided [36]. The authors used sequential UPS-XPS-UPS analysis. UPS spectra of pre-oxidized ceria revealed no  $\text{Ce}^{3+}$ . However, subsequent XPS analysis indicated a rather high concentration of  $\text{Ce}^{3+}$  ions. When the UPS spectra were taken again with the same sample,  $\text{Ce}^{3+}$  ions were detected. These results unequivocally demonstrate the photoreductive effect of X-rays on ceria, and it has been pointed out that the initial  $\text{Ce}^{3+}/\text{Ce}^{4+}$  ratio can be strongly overestimated when determined using the  $\text{Ce}^{3+}$  XPS signals. In addition, it has been recently underlined that the widespread assignment of an XPS peak at  $531\text{--}532 \text{ eV}$  to oxygen vacancies is not correct [37].

Consider now the Raman results. The most important feature in the Raman spectra of stoichiometric ceria is an intense  $F_{2g}$  mode at  $460\text{ cm}^{-1}$ . Reduction of ceria leads to the development of the so-called D1-band (D stands for defects) observed around  $550\text{ cm}^{-1}$ . This band is attributed to  $Ce^{3+}-O^{2-}-Ce^{4+}$  modes [38] and is associated with the presence of oxygen vacancies [21,28,39–41]. It disappeared after adsorption of oxygen [17,42], which confirms the assignment. Very often, another D-band (the so-called D2 band at ca.  $600\text{ cm}^{-1}$ ) is incorrectly also attributed to oxygen vacancies in ceria, which is consequently associated with the presence of reduced  $Ce^{3+}$  sites. Therefore, it may be concluded that in some of these studies, the  $Ce^{3+}/Ce^{4+}$  ratio is also strongly overestimated.

In this work, we investigate the reoxidation by  $O_2$  of ceria nanoshapes reduced at 773 K. This temperature ensures that mainly  $Ce^{4+}$  cations on the surface are reduced and prevents morphological changes in the samples. We first analyzed the  $Ce^{3+}$  electronic band appearing at  $2133\text{--}2095\text{ cm}^{-1}$  and found that it possesses a fine structure that is better resolved at 100 K. We have shown that  $O_2$  readily oxidizes a large fraction of  $Ce^{3+}$  to  $Ce^{4+}$  even at 100 K. Some residual  $Ce^{3+}$  sites resist the fast oxidation even in the presence of gas-phase  $O_2$ , but at 400 K, the oxidation is complete. Furthermore, we found that hydrogen dissolved in ceria is also oxidized, some of it even at 100 K, indicating its high reactivity.

## 2. Results

### 2.1. Initial Characterization of the Samples

We have studied three ceria samples prepared using hydrothermal synthesis and differing in morphology: nanocubes, nanorods, and nanoparticles. Some basic characteristics, as well as the notation of the samples that will be used further on in the text, are presented in Table 1.

**Table 1.** Some characteristics of the samples studied.

Sample	Particle Shape	$S_{BET},\text{ m}^2\text{ g}^{-1}$	Mean Crystallite Size, nm <sup>1</sup>
CeO <sub>2</sub> -NC	cubes	27	30
CeO <sub>2</sub> -NR	rods	110	7
CeO <sub>2</sub> -NP	polyhedra	140	7

<sup>1</sup> Average particle size determined according to Scherrer's equation.

#### 2.1.1. TEM Studies

TEM images of the investigated samples are shown in Figure 1. The CeO<sub>2</sub>-NC sample consists of agglomerates of nanoparticles with a cubic morphology and a typical particle size of ca. 30–35 nm, although smaller particles also exist (Figure 1a). A few particles with a polyhedral, sphere-like morphology were also noticed. Analysis showed that mainly {100} facets were exposed on the sample surface, while {111} and {110} facets were found to a small extent. The nanorods (CeO<sub>2</sub>-NR) are between 80 and 140 nm in length and about 8 nm in diameter (Figure 1b). With this sample, the most exposed facets are {110} and {111}, while only a small fraction of {100} facets was detected. The CeO<sub>2</sub>-NP sample is composed of polyhedral nanoparticles with a size of 2–8 nm (Figure 1c). They are packed randomly with {100}, {110} and {111} lattice fringes. In this case, the presence of traces of nanorods was also noticed.

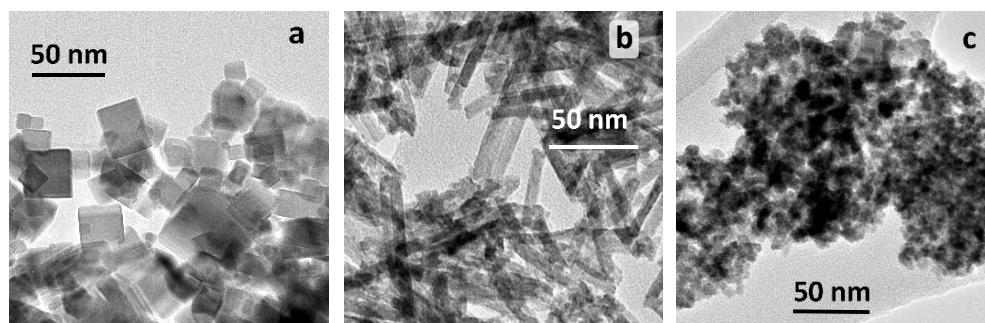


**Figure 1.** TEM photographs of CeO<sub>2</sub>-NC (a), CeO<sub>2</sub>-NR (b), and CeO<sub>2</sub>-NP (c).

### 2.1.2. XRD Studies

Figure 2 presents the XRD patterns of our ceria samples. CeO<sub>2</sub>-NC shows sharp peaks at 28.5°, 33.0°, 47.4°, 56.2°, 59.1°, 69.4°, 76.7° and 79°. These peaks are attributed to the (111), (200), (220), (311), (222), (400), (331), and (420) Miller indices of the cubic fluorite structure of CeO<sub>2</sub> (CaF<sub>2</sub> structural type, space group Fm3m) according to the ICSD file 53,995.

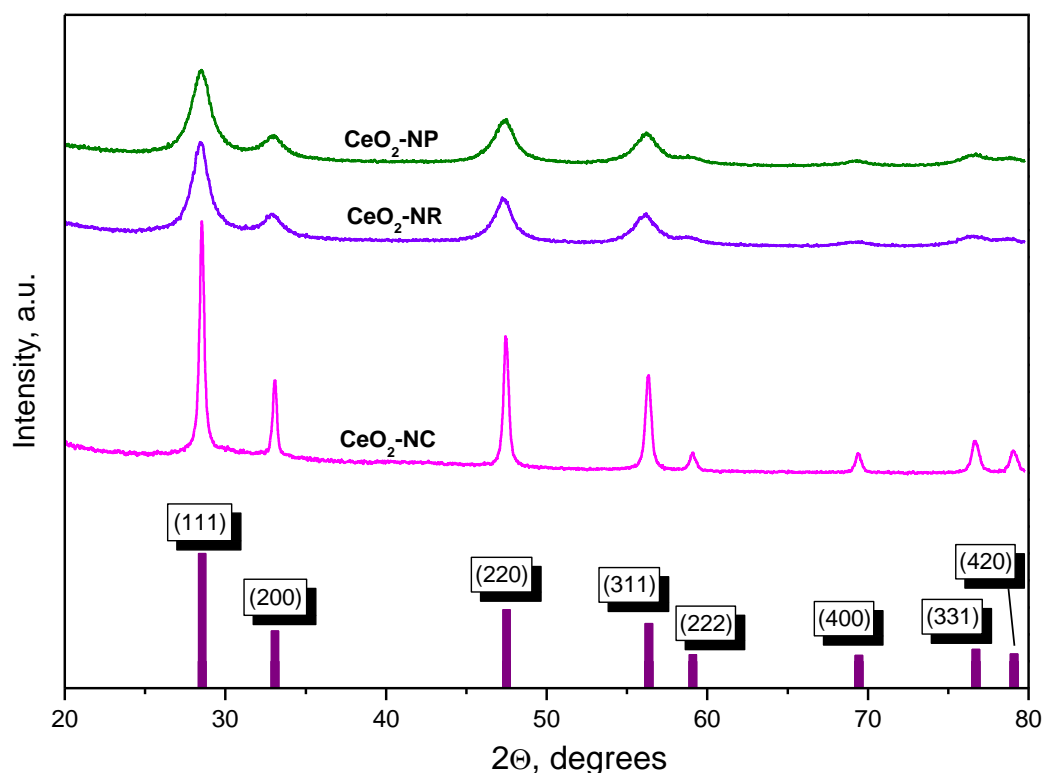


**Figure 2.** XRD patterns of CeO<sub>2</sub>-NC, CeO<sub>2</sub>-NR, and CeO<sub>2</sub>-NP. Data from the ICSD file 53,995 are shown at the bottom for comparison.

The XRD patterns of CeO<sub>2</sub>-NP and CeO<sub>2</sub>-NR are very similar. Compared to the CeO<sub>2</sub>-NC sample, the peaks are broader, which is consistent with the smaller particle size and higher specific surface area of these two samples.

### 2.1.3. TPR Studies

The TPR profiles obtained with the ceria samples (Figure 3) are in general agreement with previous findings [8–14]. The CeO<sub>2</sub>-NR and CeO<sub>2</sub>-NP samples show similar TPR profiles. The bulk reduction is associated with the peaks at 1103–1116 K, where surface reduction gives rise to composite peaks below 900 K. Computer deconvolution suggests

that the low-temperature peaks consist of at least four components each. In addition, a negative peak around 870 K is also detected with both samples. This peak was attributed to the desorption of  $H_2$  [10,43]. However, reduction of residual surface carbonates and release of CO could also contribute to the peak, as proposed by Perrichon et al. [9]. Indeed, some carbonates were detected using IR spectroscopy with all samples (see below).

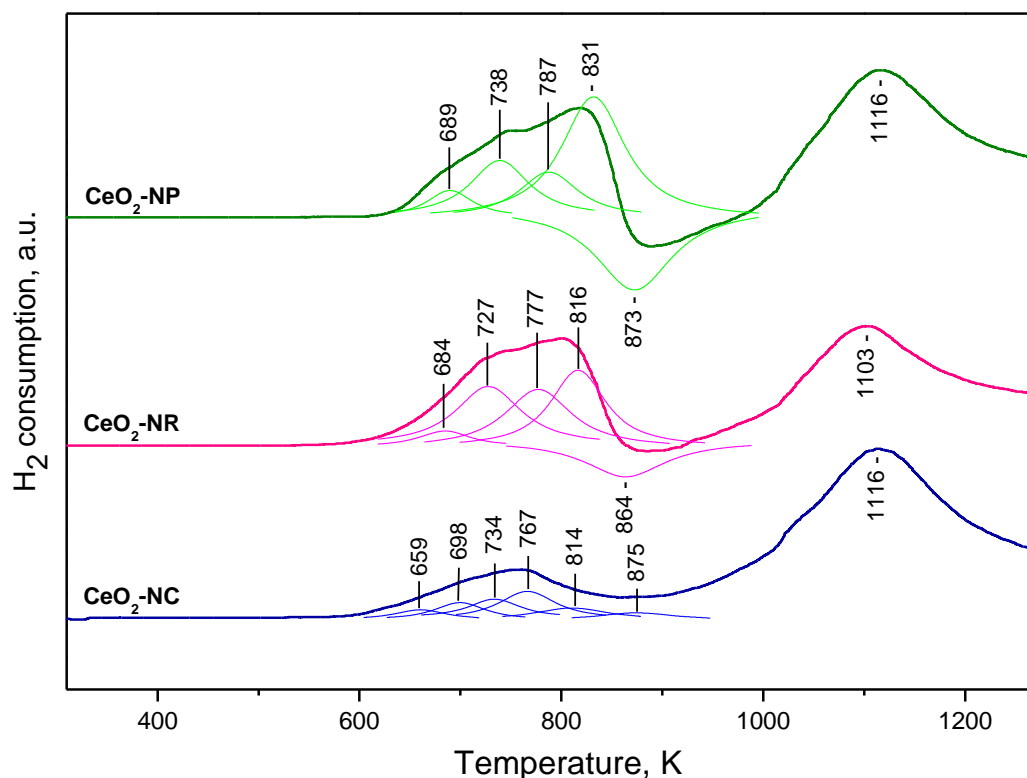


**Figure 3.**  $H_2$ -TPR profiles of  $CeO_2$ -NC,  $CeO_2$ -NR and  $CeO_2$ -NP.

The surface of the  $CeO_2$ -NC sample is more easily reduced. It is characterized by a less intense first peak, which is consistent with the lower specific surface of this sample. The peak appears at ca. 760 K, i.e., at a temperature lower than that for the  $CeO_2$ -NP and  $CeO_2$ -NR samples. It also has a complex character. The second peak attributed to bulk reduction is registered at 1116 K. No negative peak was discernible with this sample. However, we cannot rule out the possibility of its existence and cancelation by a positive peak around this temperature.

Data on the hydrogen consumption below and above 923 K for the different samples are provided in the Supporting Materials (Table S1).

## 2.2. Background IR Spectra of Oxidized and Reduced Samples

### 2.2.1. $CeO_2$ -NC

The FTIR spectra of activated and reduced  $CeO_2$ -NC samples are compared in Figure 4. The activated sample is characterized by a typical oxidized ceria hydroxyl spectrum (see the left inset in Figure 4): a band at  $3723\text{ cm}^{-1}$  is assigned to terminal  $Ce^{4+}$ -OH groups, while the bands at  $3653$  and  $3635\text{ cm}^{-1}$  correspond to bridging hydroxyls [23,24,27,44]. A weak composite band at  $3511\text{ cm}^{-1}$  is also visible. It is often attributed to the oxy-hydroxide phase [23,24,27,44] or triply bridging OH groups [27,44]. We support the former assignment because the frequency is too low for bridging species [45] and indicates that the hydroxyls are H-bonded. In the low-frequency region, two sharp bands at  $1460$  and  $1384\text{ cm}^{-1}$  and weaker bands at  $1068$  and  $857\text{ cm}^{-1}$  are detected. These bands are attributed to residual carbonate species [46].

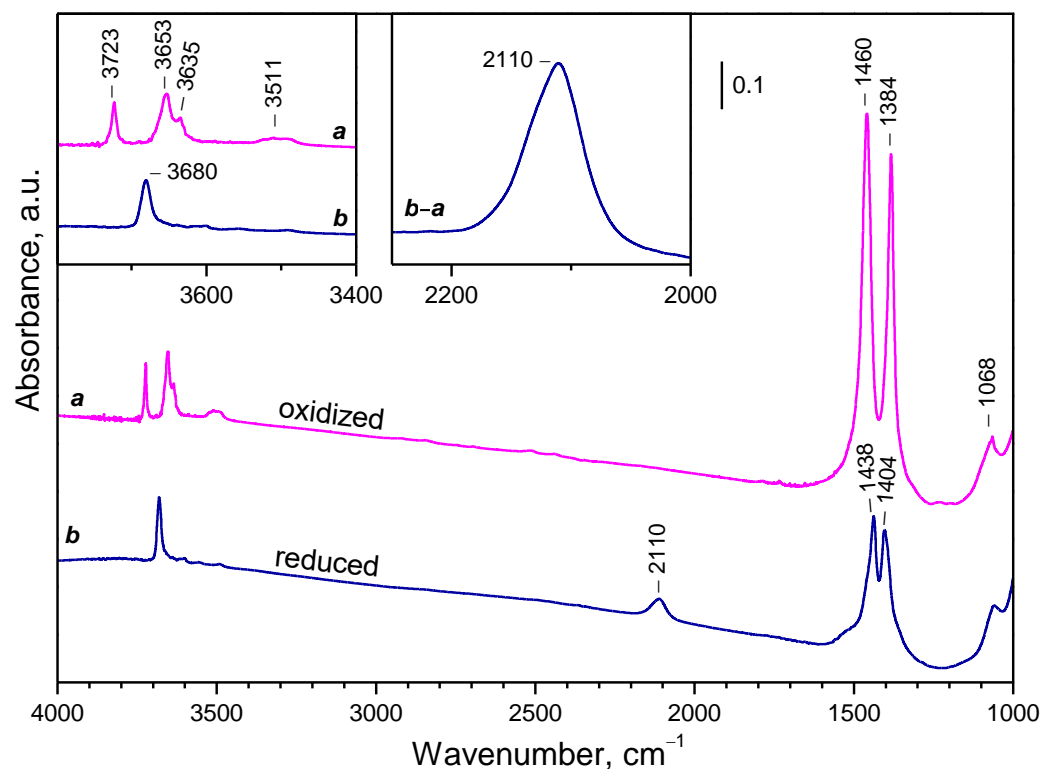


**Figure 4.** FTIR spectra of CeO<sub>2</sub>-NC after activation (a) and reduction (b) at 773 K.

Reduction at 773 K, followed by evacuation at the same temperature, leads to specific changes in the IR spectrum. First, the bands due to linear and bridging OH groups disappeared, and a new hydroxyl band appeared at 3680 cm<sup>-1</sup>. This band is typical of bridging hydroxyls on reduced ceria [10,24,47]. The bands of H-bonded hydroxyls (around 3500 cm<sup>-1</sup>) strongly decreased in intensity. This also happened with the carbonate bands at 1460 and 1384 cm<sup>-1</sup>, which also shifted to become closer to each other. This smaller band split is characteristic of higher symmetry of related carbonates [46]. It was also noticed that the carbonate bands slightly decreased in intensity after each reoxidation/reduction step. Finally, a new band at 2110 cm<sup>-1</sup> emerged (see the right inset in Figure 4). This band is assigned to the <sup>2</sup>F<sub>5/2</sub> → <sup>2</sup>F<sub>7/2</sub> electronic transition of Ce<sup>3+</sup> [20,22–27] and is used in what follows to estimate the reduction degree of our samples. The band has a complex contour, and computer deconvolution suggests it consists of several components. We have also estimated that the detection limit for Ce<sup>3+</sup> in our experiments with this sample is ca. 0.03% of the total amount of cerium cations.

### 2.2.2. CeO<sub>2</sub>-NR and CeO<sub>2</sub>-NP

The FTIR spectra of the CeO<sub>2</sub>-NR sample (Figure S1) slightly differ from those of the CeO<sub>2</sub>-NC. With the oxidized sample, the band due to terminal OH groups is of negligible intensity, while the hydroxyl spectrum of the reduced sample is more complex. Carbonate bands were of lower intensity and detected at 1573, 1486, 1353, 1292 and 1068 cm<sup>-1</sup>. For the reduced sample, only two main bands were observed at 1459 and 1371 cm<sup>-1</sup>, i.e., again, they became closer in positions. The Ce<sup>3+</sup> electronic band is composite, but the main component appears to be at 2128 cm<sup>-1</sup>.

The spectra of CeO<sub>2</sub>-NP (Figure S2) are rather similar to the spectra of CeO<sub>2</sub>-NR. The main difference is the existence of both oxidized and reduced samples of a broad band centered at ca. 3400 cm<sup>-1</sup>, which is attributed to occluded H-bonded hydroxyl groups.

Finally, we estimated the coverage by residual carbonates. For that purpose, we adsorbed CO<sub>2</sub> under 2 mbar equilibrium pressure on CeO<sub>2</sub>-NP and then evacuated the gas phase at ambient temperature. The carbonate bands produced in the 1700–1200 cm<sup>-1</sup>

region were too intense to be followed accurately. However, the deformation modes at  $858\text{ cm}^{-1}$  appeared with optimal intensity, and it was found that the residual carbonates accounted for ca. 6% of the total amount of carbonates produced after  $\text{CO}_2$  adsorption. Therefore, we may conclude that only a small part of the activated sample is covered by carbonates.

### 2.2.3. Oxidation of Reduced Ceria by Different Reagents

It has been reported that reduced ceria surface can be easily re-oxidized at ambient temperature by  $\text{O}_2$ ,  $\text{NO}$ , and  $\text{N}_2\text{O}$  [25]. However, there are reports describing its oxidation by  $\text{CO}_2$  and  $\text{H}_2\text{O}$  [48]. Although in the latter two cases, the process is considered to proceed at high temperature, we have checked the stability of  $\text{Ce}^{3+}$  in the presence of  $\text{H}_2\text{O}$  and  $\text{CO}_2$  at room temperature. The results showed that no oxidation occurs under these conditions (Figure S3). Only a large amount of water caused erosion of the  $\text{Ce}^{3+}$  band, but it was fully recovered after subsequent evaluation at 773 K.

### 2.2.4. Temperature Changes of the IR Spectra

It is known that lowering the temperature could lead to better resolution of superimposed bands. Figure 5 compares the spectra in the region of  $\text{Ce}^{3+}$  electronic transition of reduced samples registered at RT, and at 100 K. First, the  $\text{Ce}^{3+}$  band increases in intensity at low temperatures. Secondly, several components become well-resolved. The low-frequency components ( $2105$  and  $2094\text{ cm}^{-1}$ ) are emphasized for the  $\text{CeO}_2\text{-NC}$  sample, which may suggest that they are associated with the  $\{100\}$  facets.

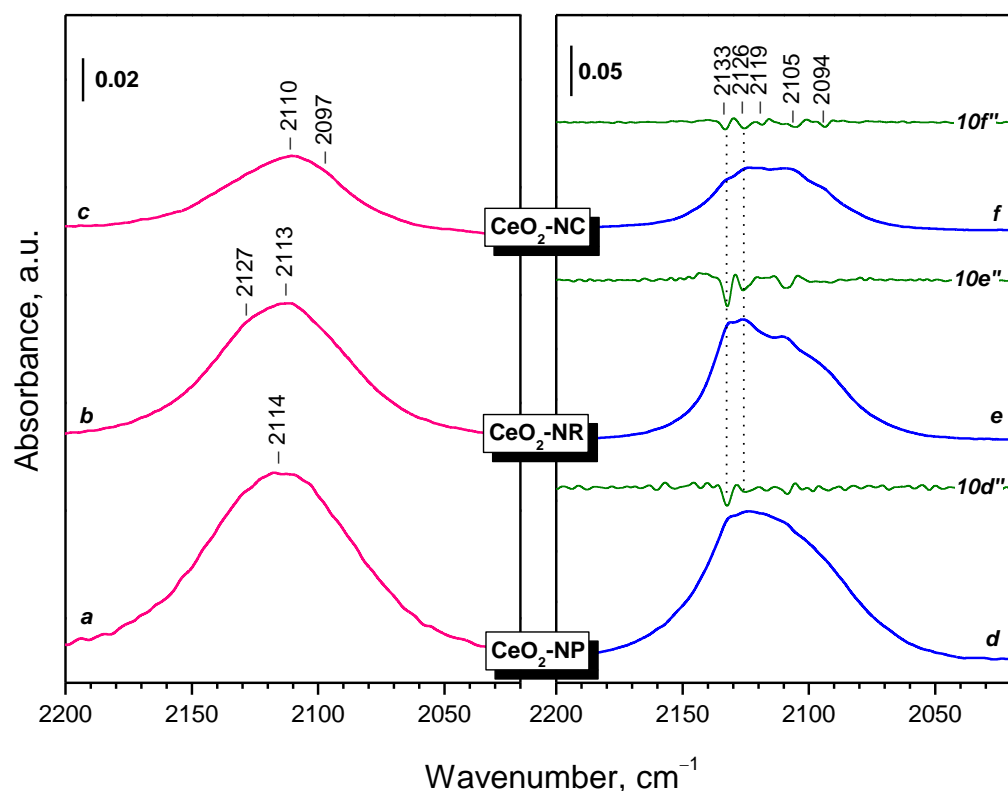


**Figure 5.** FTIR spectra of reduced ceria samples in the region of  $\text{Ce}^{3+}$  electronic transition:  $\text{CeO}_2\text{-NP}$  (a,d),  $\text{CeO}_2\text{-NR}$  (b,e), and  $\text{CeO}_2\text{-NC}$  (c,f). Spectra (a–c) are registered at ambient temperature, while spectra (d–f) are at 100 K. The second derivatives of the spectra (d–f) are multiplied by a factor of 10 and are denoted as  $10d''$ ,  $10e''$  and  $10f''$ . All spectra are baseline-corrected.

The hydroxyl spectra, and to a smaller extent, the carbonate bands, are also affected by temperature (see Figure S4).

### 2.3. Interaction of Activated Samples with O<sub>2</sub> at Variable Temperatures

Although most authors are of the opinion that reactive oxygen adsorption on ceria occurs on reduced Ce<sup>3+</sup> cations, there are also opinions that the adsorption sites are Ce<sup>4+</sup> cations [33,34]. In order to check this, we have studied O<sub>2</sub> adsorption on activated (oxidized) samples. No Ce<sup>3+</sup> electronic band was detected for CeO<sub>2</sub>-NC samples activated at 573, 673, and 773 K, indicating the lack of Ce<sup>3+</sup> sites. Adsorption of O<sub>2</sub> (2 mbar equilibrium pressure) at 100 K on these samples after each of these pretreatments led only to the appearance of a weak band at 1555–1553 cm<sup>-1</sup> attributed to molecularly adsorbed O<sub>2</sub> (Figure S5), in agreement with previous studies. The O<sub>2</sub> band increases in intensity with the activation temperature of ceria due to dehydroxylation and the creation of Ce<sup>4+</sup> Lewis acid sites. Warming the sample up to ambient temperature leads only to the fast disappearance of this band. The same situation was found with the other two samples. Therefore, we conclude that molecular adsorption of O<sub>2</sub> proceeds on Ce<sup>4+</sup> sites, and for reactive O<sub>2</sub> adsorption, Ce<sup>3+</sup> sites are necessary.

### 2.4. Interaction of Reduced CeO<sub>2</sub>-NC with O<sub>2</sub> at Variable Temperature

In order to follow the initial stages of ceria reoxidation, we studied the interaction of reduced samples at 100 K, followed by a gradual increase in the temperature. For the unambiguous assignment of the peaks, we also performed experiments with <sup>18</sup>O<sub>2</sub>.

#### 2.4.1. Interaction with <sup>16</sup>O<sub>2</sub>

The background spectrum of CeO<sub>2</sub>-NC registered at 100 K is shown in Figure 6, spectrum a. As already discussed, the intensity of the Ce<sup>3+</sup> electronic band is enhanced as compared to the spectrum registered at ambient temperature. The hydroxyl and carbonate bands are slightly shifted. The introduction of O<sub>2</sub> (2 mbar) to the sample leads to an immediate substantial drop in the intensity of the Ce<sup>3+</sup> electronic band (Figure 6, spectrum b). Difference spectra (a–b) indicate that the band was substantially eroded from the higher and lower frequency sides. This indicates the lack of correlation between the band position and the reactivity of the related species. According to the integral band area, 45% of the Ce<sup>3+</sup> sites were immediately oxidized. No further measurable changes occurred when the sample was allowed to stay in the O<sub>2</sub> atmosphere at 100 K for 10 min.

In the ν(OH) region (Figure 6, panel B), the band at 3685 cm<sup>-1</sup> practically disappeared, and a new band (typical of the oxidized sample) appeared at 3653 cm<sup>-1</sup>. The band at 3503 cm<sup>-1</sup> remained intact. The results indicate that all Ce<sup>3+</sup> sites bound to OH species (3685 cm<sup>-1</sup>) are very rapidly oxidized.

A band at 1127 cm<sup>-1</sup> developed upon O<sub>2</sub> exposure (Figure 6, panel C) and is attributed to the ν(O–O) modes of superoxo (O<sub>2</sub><sup>-</sup>) species [32–34]. The respective overtone was detected at 2237 cm<sup>-1</sup> (see Figure 6, pane A). This indicates that oxidation of Ce<sup>3+</sup> with the formation of Ce<sup>4+</sup>–O<sub>2</sub><sup>-</sup> species takes place.

It should also be noted that weak bands developed in the 900–800 cm<sup>-1</sup> region and could characterize peroxy species. However, the strong background changes in this region during reoxidation hinder the exact assignments. For proper assignment of these bands, we further explored the adsorption of isotopically labeled oxygen, <sup>18</sup>O<sub>2</sub> (see below).

Finally, a weak band at 1553 cm<sup>-1</sup>, also detected with the oxidized sample, appeared with reduced intensity. The band is of very weak stability and was already attributed to molecularly adsorbed O<sub>2</sub>. It will not be discussed further on.

As the temperature increased, the Ce<sup>3+</sup> electronic band progressively faded and disappeared at 373 K. The intensity of the superoxide band initially slightly increases (Figure 6, spectra c, d) and then starts to decrease, with the band disappearing at 400 K (Figure 6, spectra e–k). The OH band is slightly red-shifted to 3651 cm<sup>-1</sup>, and weak components due to terminal hydroxyls (3722 and 3705 cm<sup>-1</sup>) developed at 400 K.

Note that the intensity changes and the band shifts in the experiments performed at different temperatures should be taken with care. First, the decrease in the Ce<sup>3+</sup> band in intensity is partly due to temperature increase. The shift and the slight decrease in intensity

of the OH band at  $3633\text{ cm}^{-1}$  should also be mainly related to temperature change, and this most probably applies to the position of the superoxide band.

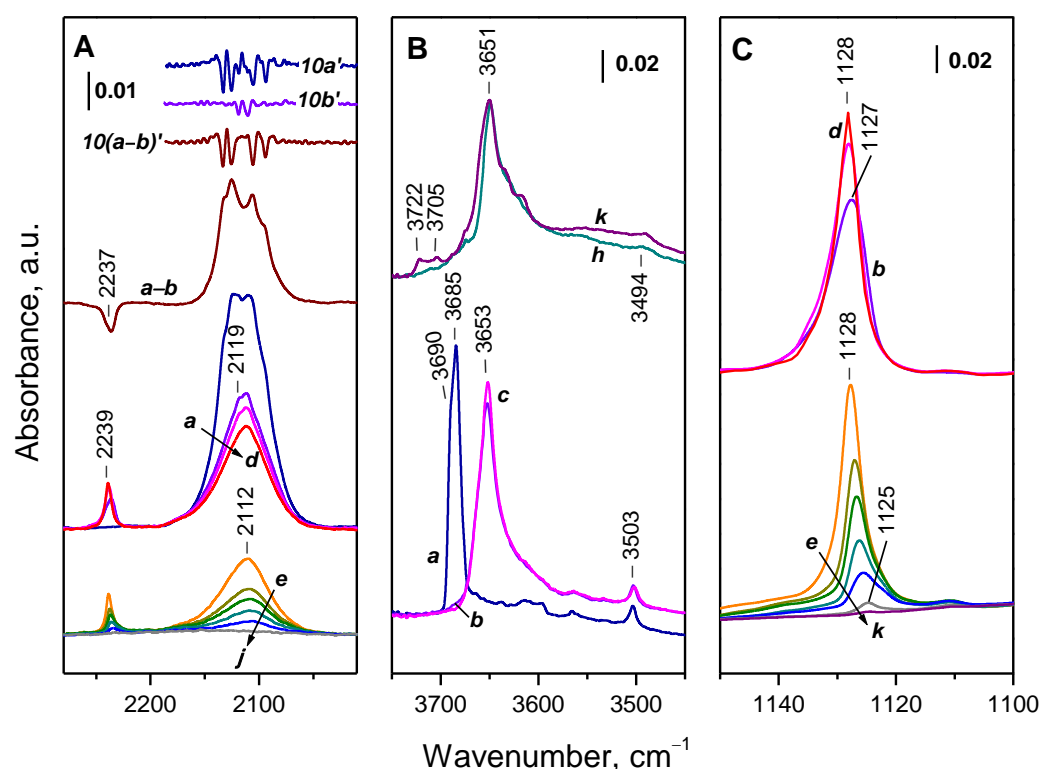


**Figure 6.** FTIR spectra of reduced  $\text{CeO}_2\text{-NC}$  were recorded at 100 K (a), after the addition of 2 mbar  $\text{O}_2$  at 100 K (b), a gradual increase in temperature up to ambient one (c–h), and after 5 min. heating the sample in the oxygen atmosphere at 323 K (i), 373 K (j), and 400 K (k). (A) shows the region of  $\text{Ce}^{3+}$  electronic transition, and the spectra are baseline corrected. Some second derivatives are shown at the top part of the panel. (B) shows the hydroxyl stretching region. (C) presents the spectra in the  $\nu(\text{O-O})$  region of the superoxide anion, and the spectra are background-corrected.

#### 2.4.2. Interaction with $^{18}\text{O}_2$

To confirm the proposed assignments of bands to superoxo and peroxo species, we performed experiments with  $^{18}\text{O}_2$ . In order to obtain more information on the elementary reaction steps, we first studied successive adsorption of small doses of  $^{18}\text{O}_2$  (Figures 7 and 8).

Difference spectra presented in Figure 7 shows that with the increase in the amount of  $^{18}\text{O}_2$  introduced into the IR cell, four components of the  $\text{Ce}^{3+}$  electronic band, at 2133, 2126, 2105, and  $2095\text{ cm}^{-1}$ , disappear almost simultaneously.

The band at  $1128\text{ cm}^{-1}$  observed after adsorption of  $^{16}\text{O}_2$  was not detected, but a band at  $1064\text{ cm}^{-1}$  developed instead. The isotopic shift factor of 1.06 is in excellent agreement with the expectation for the  $\nu(\text{O-O})$  modes. This confirms the assignment of the  $1128\text{ cm}^{-1}$  band to  $\text{O}_2^-$  species and also shows that no  $(^{16}\text{O}^{18}\text{O})^-$  species were produced during the experiments. As expected, the overtone of the  $^{16}\text{O}_2^-$  band was also missing. According to the isotopic shift factor, it should be observed at  $2110\text{ cm}^{-1}$  but is superimposed with the  $\text{Ce}^{3+}$  band. Therefore, one should consider that a small contribution of the overtone as a positive band exists in the spectra presented in the left panel of Figure 7 (position marked with red segment).

Consider now the region where peroxide species are expected to absorb. The analysis is complicated because of the shift of the background band at ca.  $865\text{ cm}^{-1}$  during sample oxidation and the sample cut-off around  $870\text{ cm}^{-1}$ . However, a comparison of the spectra of adsorbed  $^{16}\text{O}_2$  and  $^{18}\text{O}_2$  (Figure 8) allows for making definite conclusions. For convenience, the results are summarized in Table 2.

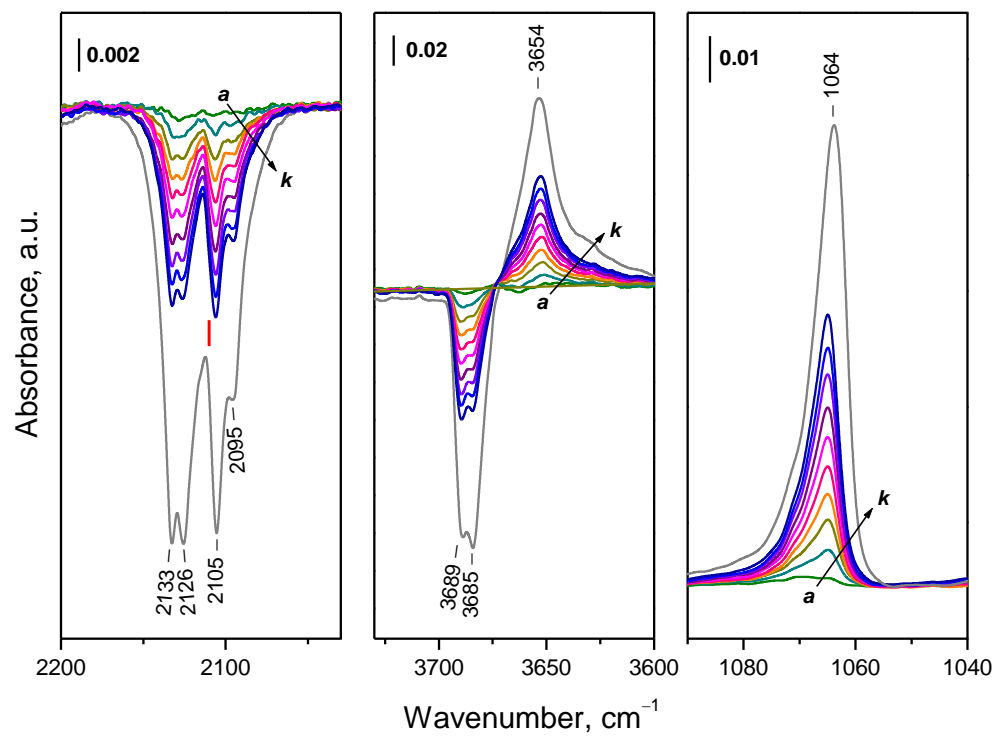


**Figure 7.** FTIR spectra were recorded after successive adsorption of small doses of  $^{18}\text{O}_2$  at 100 K on a reduced  $\text{CeO}_2\text{-NC}$  sample (a–j) and after saturation in the presence of 2 mbar  $\text{O}_2$  (k).

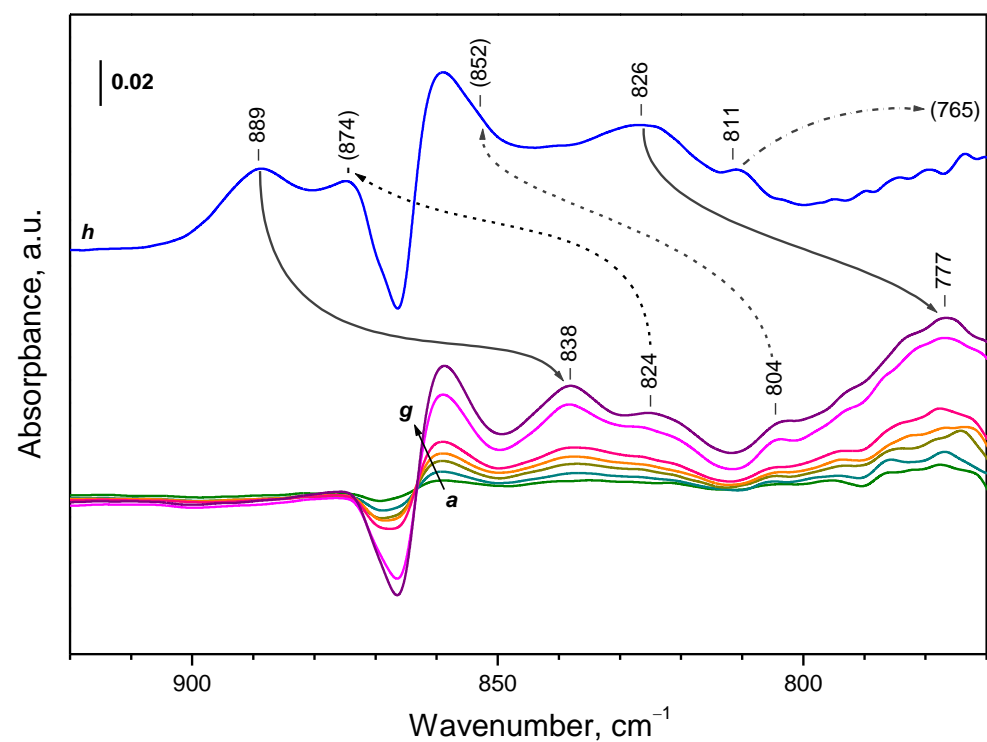


**Figure 8.** Selected FTIR spectra were recorded after successive adsorption of small doses of  $^{18}\text{O}_2$  at 100 K on a reduced  $\text{CeO}_2\text{-NC}$  sample (a–f), in the presence of 2 mbar  $^{18}\text{O}_2$  (g) and in the presence of 2 mbar  $^{16}\text{O}_2$  (h).

**Table 2.** Positions of  $^{16}\text{O}$  and  $^{18}\text{O}$  superoxide and peroxide bands on  $\text{CeO}_2\text{-NC}$  and  $\text{CeO}_2\text{-NP}$  samples.

Sample	Assignment	$\nu(^{16}\text{O}\text{-}^{16}\text{O}), \text{cm}^{-1}$	$\nu(^{18}\text{O}\text{-}^{18}\text{O}), \text{cm}^{-1}$	$i^1$
$\text{CeO}_2\text{-NC}$	superoxide	1128	1064	1060
$\text{CeO}_2\text{-NC}$	superoxide	1160	1093	1061
$\text{CeO}_2\text{-NP}$	superoxide	1128	1065	1059
$\text{CeO}_2\text{-NP}$	superoxide	1137	1072	1061
$\text{CeO}_2\text{-NC}$	peroxide	889	838	1061
$\text{CeO}_2\text{-NC}$	peroxide	874	824	1061
$\text{CeO}_2\text{-NC}$	peroxide	852	804	1060
$\text{CeO}_2\text{-NC}$	peroxide	826	777	1063
$\text{CeO}_2\text{-NC}$	peroxide	811	765 <sup>2</sup>	-
$\text{CeO}_2\text{-NP}$	peroxide	889	840	1058

<sup>1</sup> Isotopic shift factor. <sup>2</sup> Calculated value.

First, the two most intense bands at 889 and 826  $\text{cm}^{-1}$ , produced after  $^{16}\text{O}_2$  adsorption, are shifted to 838 and 777  $\text{cm}^{-1}$ , respectively, when  $^{18}\text{O}_2$  was utilized (isotopic shift factor 1.06). Two more bands, at 874 and 852  $\text{cm}^{-1}$ , are not well discernible in the spectra of adsorbed  $^{16}\text{O}_2$  but are well detected after adsorption of  $^{18}\text{O}_2$  at 824 and 804  $\text{cm}^{-1}$ , respectively. Another band at 811  $\text{cm}^{-1}$  was observed only after adsorption of  $^{16}\text{O}_2$ , and the position of the respective  $^{18}\text{O}_2$  band was below the sample cut-off. All these bands are assigned to different peroxide species, and all of them develop almost in concert.

Analysis of the hydroxyl region (Figure 7) shows that the OH bands associated with a reduced surface (3689 and 3685  $\text{cm}^{-1}$  at 100 K) are eroded in parallel with the components of the  $\text{Ce}^{3+}$  band and a new band at 3654  $\text{cm}^{-1}$  (typical of the oxidized surface) develops at their expense. The superoxide band at 1065  $\text{cm}^{-1}$  and the peroxide bands also grow almost in parallel with these changes. The same is valid for the shift of the carbonate bands (Figure S6). The results show that the fast ceria oxidation at 100 K includes oxidation of all  $\text{Ce}^{3+}$  sites bound to OH groups and carbonate anions. Note, however, that this does not exclude the possibility of parallel oxidation processes, including  $\text{Ce}^{3+}$  sites that are not bound to OH groups and/or carbonates.

An increase in temperature in the presence of 2 mbar  $^{18}\text{O}_2$  leads to changes similar to those described in the experiments with  $^{16}\text{O}_2$ , although all oxygen bands were shifted. Here, we shall only discuss the peroxide bands (Figure 9) because they were not discussed in the previous section.

The band at 889  $\text{cm}^{-1}$  was hardly affected when the temperature was raised from 100 K to ambient one. Only a small decrease in intensity and red-shift were noticed. However, the intensity of this band is substantially reduced after heating at 373 K (Figure 9, spectrum e). At this temperature, the band at 826  $\text{cm}^{-1}$  disappears. This means that the respective peroxide species decompose between ambient temperature and ca 373 K. In contrast, the band at 810  $\text{cm}^{-1}$  developed, and this was more pronounced after heating at 373 K. In this case, a shoulder at 817  $\text{cm}^{-1}$  becomes also well visible. The intensities of the other peroxide bands were too low to follow them accurately.

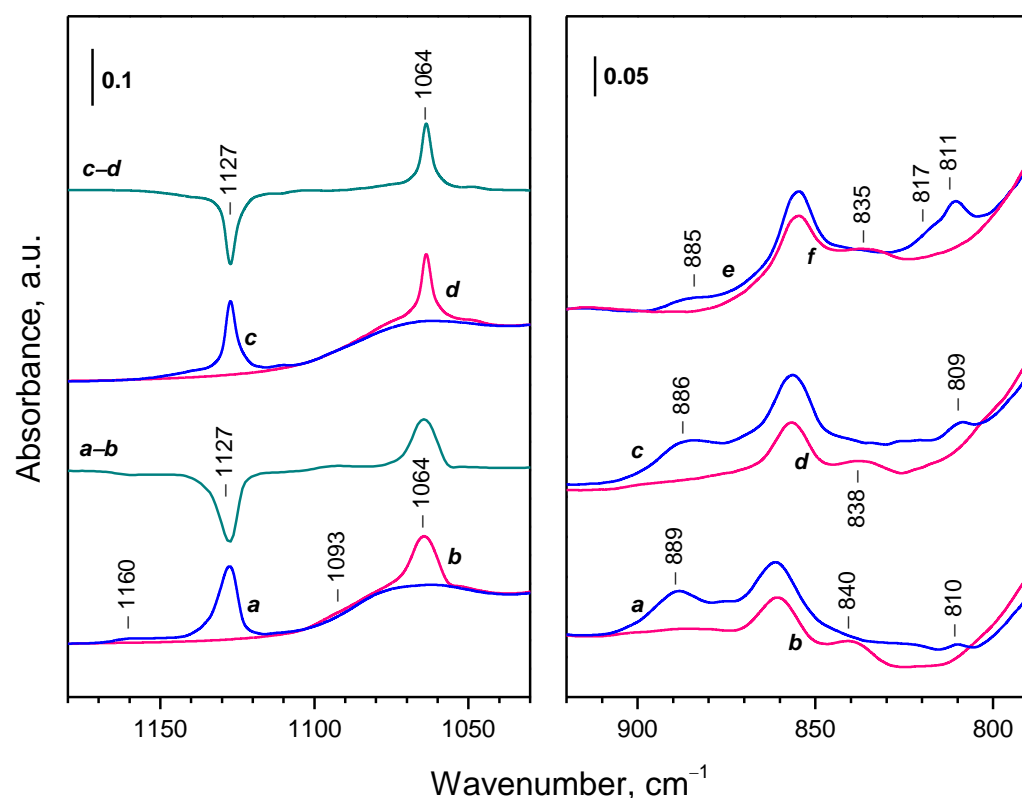


**Figure 9.** FTIR spectra of reduced CeO<sub>2</sub>-NC registered after interaction with <sup>16</sup>O<sub>2</sub> (a,c,e) or <sup>18</sup>O<sub>2</sub> (b,d,f): addition of 2 mbar of <sup>16</sup>O<sub>2</sub>/<sup>18</sup>O<sub>2</sub> to the sample at 100 K (a,b) and after increase in the temperature to 298 K (c,d) and 373 K (e,f).

#### 2.4.3. Interaction of Hydroxylated CeO<sub>2</sub>-NC with <sup>16</sup>O<sub>2</sub>

In order to obtain information on how the hydroxylation degree affects the fine structure of the Ce<sup>3+</sup> electronic band and the oxidation process as a whole, we studied oxygen adsorption on a reduced sample that was evacuated only at 573 K. Preliminary experiments have shown that after this pretreatment all of the molecularly adsorbed water is eliminated (lack of  $\delta(\text{H}_2\text{O})$  band at ca. 1620 cm<sup>-1</sup>). Two principal hydroxyl bands appeared in the spectrum at 3684 and 3659 cm<sup>-1</sup>, together with two weaker features at 3615 and 3533 cm<sup>-1</sup>. In addition, a broad band centered at ca. 3300 cm<sup>-1</sup> evidences the existence of a fraction of H-bonded hydroxyls. At low temperatures, the bands shifted, and the two main bands were detected at 3690 and 3663 cm<sup>-1</sup>. The carbonate bands appeared at 1475, 1464, 1440, 1407 and 1380 cm<sup>-1</sup>. The second derivative indicated that the Ce<sup>3+</sup> band consisted mainly of three components at 2127, 2109, and 2094 cm<sup>-1</sup>.

Dosage of <sup>16</sup>O<sub>2</sub> to the sample led to a gradual development of three negative bands at 2126, 2109, and 2095 cm<sup>-1</sup>, evidencing oxidation of Ce<sup>3+</sup> sites (Figure 10). Synchronously, a superoxide band developed at 1135 cm<sup>-1</sup>. The OH band at 3693 cm<sup>-1</sup> fully disappeared, and the band at 3664 cm<sup>-1</sup> strongly decreased in intensity. Simultaneously, a band at 3654 cm<sup>-1</sup> developed together with a broad band at ca. 3200 cm<sup>-1</sup>. In parallel with this, a band at 1620 cm<sup>-1</sup>, assigned to  $\delta(\text{H}_2\text{O})$  modes, grew up (see the right inset in Figure 10).

Comparison with the experiments performed with the 773 K evacuated sample allows us to underline two important differences. First, the decrease in intensity of the Ce<sup>3+</sup> band after dosage of the same amount of O<sub>2</sub> was definitely lower. Note that this cannot be due to kinetic limitations because no changes were observed with time after adding a definite amount of doses, i.e., all of the introduced oxygen was consumed. Second, the integral areas of the negative Ce<sup>3+</sup> electronic bands in the two sets of experiments were practically identical after the introduction of 2 mbar of O<sub>2</sub> to the system, which suggests that the same amount of Ce<sup>3+</sup> sites have been fast oxidized in the two experiments. We also note that the

band around  $1553\text{ cm}^{-1}$ , due to weakly bound molecular oxygen, was not discernible even in the presence of 2 mbar  $\text{O}_2$  in the gas phase.

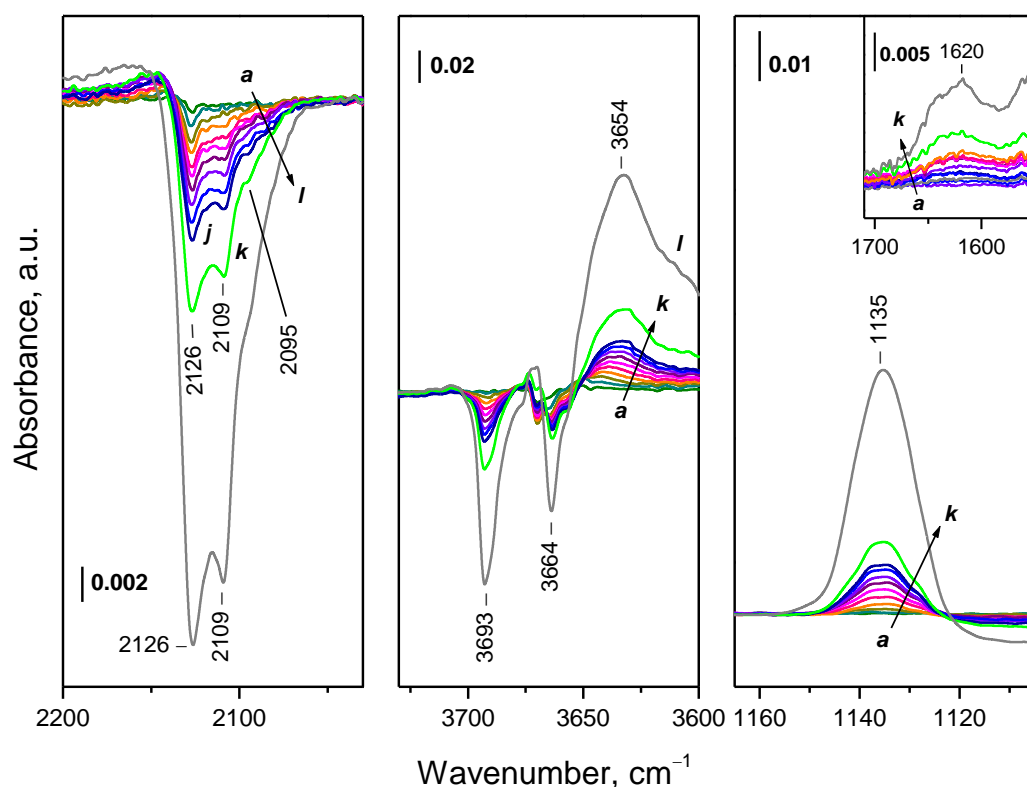


**Figure 10.** FTIR spectra were recorded after successive adsorption of small doses of  $^{16}\text{O}_2$  at 100 K on reduced  $\text{CeO}_2\text{-NC}$  sample evacuated at 573 K (a–j), after the introduction of a bigger dose (k) and in the presence of 2 mbar  $\text{O}_2$  (l).

The above findings can be rationalized assuming that part of the introduced oxygen is consumed for oxidation of  $\text{Ce}^{3+}$  sites and another part for oxidation of hydrogen dissolved in ceria. This explains the delayed development of the negative  $\text{Ce}^{3+}$  electronic band. When dissolved  $\text{H}_2$  is oxidized, water is produced and is detected by the  $\delta(\text{H}_2\text{O})$  modes and the appearance of broad absorbance in the  $\nu(\text{OH})$  region due to H-bonded water. Note that the existence of dissolved hydrogen in reduced ceria has already been reported [12,16]. Thus, the results demonstrate that hydrogen dissolved in ceria can be oxidized even at 100 K in the absence of noble metals.

During temperature increase up to ambient one, the band of the superoxide ( $1135\text{ cm}^{-1}$ ) initially slightly develops but disappears before reaching room temperature. Similar is the behavior of the  $889\text{ cm}^{-1}$  peroxide band, which appeared only at intermediate temperatures and was not practically formed at 100 K. In contrast, the low-frequency peroxide bands at  $843$  and  $830\text{ cm}^{-1}$  were much more intense on this hydroxylated sample than the sample evacuated at 773 K. Importantly, water was continuously produced up to ambient temperature. Based on the intensity of the  $\delta(\text{H}_2\text{O})$  band, it was roughly estimated that the amount of water formed at 100 K is ca. 15% of all water produced when the temperature reached ambient one.

#### 2.4.4. Interaction of $\text{CeO}_2\text{-NC}$ Reduced at Lower Temperatures with $^{16}\text{O}_2$

Finally, we studied the interaction of  $\text{O}_2$  with  $\text{CeO}_2\text{-NC}$  reduced at 623 and 673 K and then evacuated at 773 K. Figure 11 compares the spectra in the  $\text{Ce}^{3+}$  and peroxide regions of these samples with the spectra of the sample reduced at 773 K and evacuated at different temperatures.

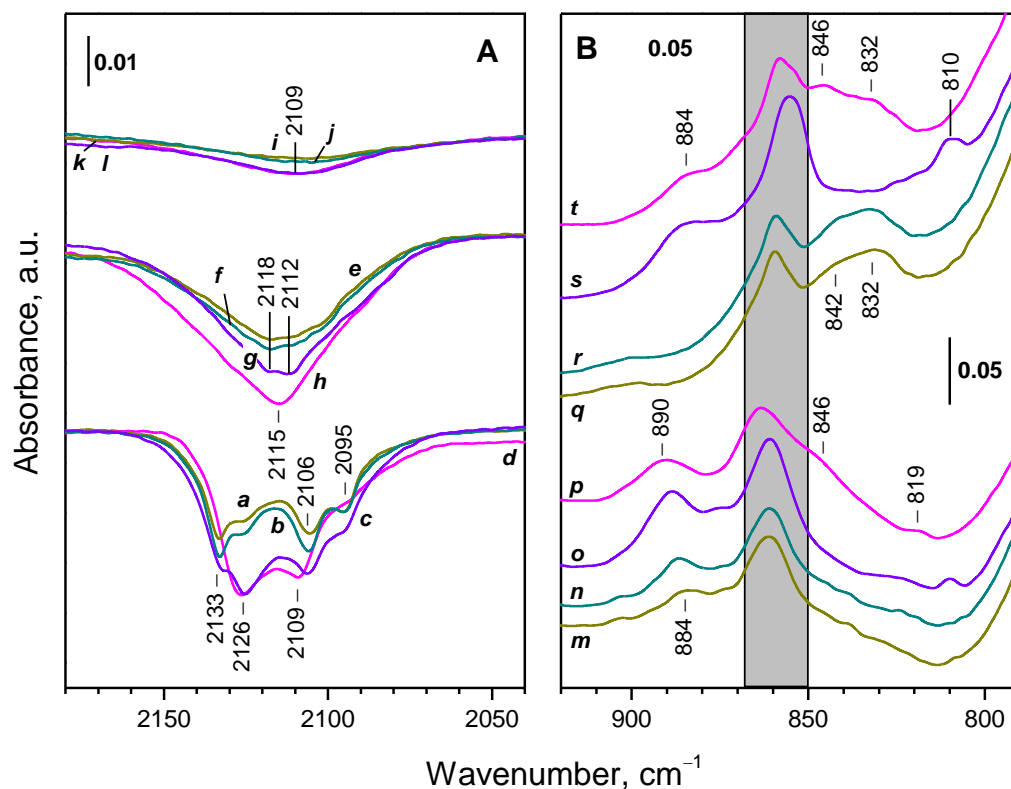


**Figure 11.** (A) Changes of the IR spectra of the CeO<sub>2</sub>-NC sample after the introduction of 2 mbar of O<sub>2</sub> at 100 K (a–d). Sample reduced at 623 K (a), 673 K (b), and 773 K (c,d); samples evacuated at 773 K (a–c) and at 573 K (d). Increase in temperature up to 293 K in the presence of O<sub>2</sub>: spectra (e–h) are recorded after spectra (a–d), respectively. Increase in temperature up to 373 K in the presence of O<sub>2</sub>: spectra (i–l) are recorded after spectra (e–h), respectively. The lower set of spectra corresponds to fast oxidation of Ce<sup>3+</sup> at 100 K, the middle set to fast oxidation between 100 K and 293 K, and the upper set to Ce<sup>3+</sup> residual to oxidation at 293 K. (B) IR spectra of CeO<sub>2</sub>-NC sample recorded after introduction of 2 mbar of O<sub>2</sub> at 100 K (m–p) and after increase in temperature to 293 K (q–t). Samples were reduced at 623 K (m,q), 673 K (n,r), and 773 K (o,p,s,t). Samples evacuated after reduction at 773 K (m,n,o,q,r,s) and at 573 K (p,t). The maxima of the peroxide species are labeled, and the grey bar shows the region of a background band.

It is seen that the reduction degree of the two samples is comparable but lower compared to the sample reduced at 773 K.

When O<sub>2</sub> interacted with the samples at 100 K, the main difference between the samples reduced at 623–673 K as compared to that reduced at 773 K is the low intensity of the negative component at 2125 cm<sup>−1</sup> (compare spectra (a) and (b) with spectrum (c) in Figure 11A). Therefore, the respective Ce<sup>3+</sup> sites are produced at higher reduction temperatures.

The spectra of the samples in the peroxide region exhibited only a weak band at 884–885 cm<sup>−1</sup>, which was more intense with the sample reduced at higher temperatures (Figure 11B, spectra m, n). Only negligible features were discernible in the 850–800 cm<sup>−1</sup> region. The superoxide band was slightly less intense compared to the 773 K reduced sample. A full conversion of OH groups and carbonate bands to the oxidized state was established.

When the temperature of the samples was gradually increased to 293 K, the main part of the residual Ce<sup>3+</sup> sites was oxidized. Two components, at 2118 and 2112 cm<sup>−1</sup>, are well discernible in the negative Ce<sup>3+</sup> electronic band (Figure 11A, spectra e, f). The same components are seen with the sample reduced at 773 K (Figure 11A, spectrum g).

The superoxide band was no longer detected at 293 K. However, intense bands due to adsorbed water appeared at  $1620\text{ cm}^{-1}$  together with a broad absorbance centered around  $3400\text{ cm}^{-1}$  (spectra not shown). The peroxide band at  $884\text{--}885\text{ cm}^{-1}$  also disappeared, and bands at  $842$  and  $832\text{ cm}^{-1}$  grew instead (Figure 11B, spectra q, r).

In this case, again, a small fraction of  $\text{Ce}^{3+}$  resisting oxidation even at 293 K was detected (Figure 11A, spectra i, j).

## 2.5. Interaction of Reduced $\text{CeO}_2\text{-NP}$ with $\text{O}_2$ at Variable Temperature

### 2.5.1. Interaction with $^{16}\text{O}_2$

As with  $\text{CeO}_2\text{-NC}$ , the introduction of  $\text{O}_2$  (2 mbar) to the reduced  $\text{CeO}_2\text{-NP}$  sample led to an immediate decrease in the intensity of the  $\text{Ce}^{3+}$  electronic band (Figure 12, spectrum b). Difference spectra show that this happens mainly at the expense of a component at  $2131\text{ cm}^{-1}$ , although some components at lower frequencies also disappeared. Based on the band intensities, it was estimated that ca. 23% of the  $\text{Ce}^{3+}$  sites have been oxidized at the conditions applied. This fraction is about two times lower than the  $\text{CeO}_2\text{-NC}$  sample. No noticeable changes occurred in the next 10 min, i.e., further oxidation at 100 K was restricted.

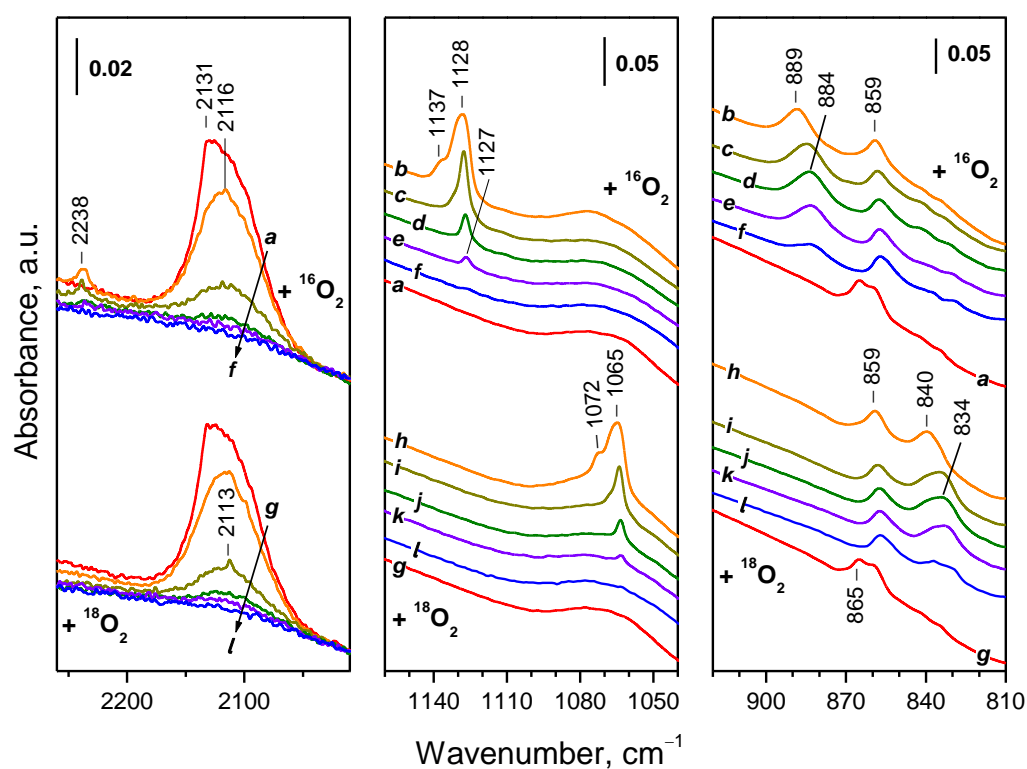


**Figure 12.** FTIR spectra of reduced  $\text{CeO}_2\text{-NP}$  registered at 100 K (a,g) and after interaction with  $^{16}\text{O}_2$  (b–f) or  $^{18}\text{O}_2$  (h–l): addition of 2 mbar of  $^{16}\text{O}_2/^{18}\text{O}_2$  to the sample at 100 K (b,h) after gradual increase in temperature (c,i), at ambient temperature (d,j) and after interaction with  $\text{O}_2$  at 323 K (e,k) and 373 K (f,l).

Simultaneously with the erosion of the  $\text{Ce}^{3+}$  electronic band, bands due to adsorbed superoxide and peroxide species emerged. The  $\nu(\text{O-O})$  band of the  $\text{O}_2^-$  species was detected at  $1128\text{ cm}^{-1}$ , and the second derivatives clearly revealed two more components at  $1131$  and  $1137\text{ cm}^{-1}$ . The peroxide species were homogeneous and characterized by a  $\nu(\text{O-O})$  band at  $889\text{ cm}^{-1}$ . In addition, the carbonate band at  $859\text{ cm}^{-1}$  gained intensity, and the band at  $865\text{ cm}^{-1}$  (indicative of carbonates on a reduced surface) disappeared. A slight development of the background band at ca.  $1070\text{ cm}^{-1}$  was also noticed.

An increase in the temperature up to ambient one led to a strong reduction and almost full disappearance of the  $\text{Ce}^{3+}$  band (Figure 12, spectra c, d), i.e., additional oxidation occurred at temperatures higher than 100 K. The band at  $1128\text{ cm}^{-1}$  initially slightly developed with temperature increase at the expense of the component at  $1137\text{ cm}^{-1}$  (spectra not shown), and then the higher-frequency components disappeared, and the  $1227\text{ cm}^{-1}$  band strongly decreased in intensity. The peroxide band slightly developed and shifted to  $884\text{ cm}^{-1}$  when the temperature increased.

Heating in oxygen at 323 and 373 K resulted in almost complete and then ultimate disappearance of the  $\text{Ce}^{3+}$  band (Figure 12, spectra e, f) and the band characterizing adsorbed  $\text{O}_2^-$  species ( $1127\text{ cm}^{-1}$ ). In contrast, the peroxide species ( $884\text{ cm}^{-1}$ ) were stable at 323 K, but their band was significantly eroded at 373 K.

### 2.5.2. Interaction with $^{18}\text{O}_2$

The changes in the spectra of the reduced  $\text{CeO}_2\text{-NP}$  sample after adsorption of  $^{18}\text{O}_2$  are identical to those already described for  $^{16}\text{O}_2$  adsorption, except for the red-shift of several bands (Figure 12). This demonstrates the good reproducibility of the experiments.

First, we note the shift of the weak band at  $2238\text{ cm}^{-1}$  in the region of the  $\text{Ce}^{3+}$  electronic transition. Indeed, a band at  $2113\text{ cm}^{-1}$  is discernible in the spectrum (i) from Figure 12.

The  $^{18}\text{O}_2^-$  principal band was detected at  $1065\text{ cm}^{-1}$ , again in line with the theoretical expectations (Figure 12, spectrum h). The same is valid for the peroxide band detected at  $840\text{--}834\text{ cm}^{-1}$  (Figure 12, spectra h and j, respectively).

If the weak component around  $1070\text{ cm}^{-1}$  was due to adsorbed dioxygen, a band around  $1010\text{ cm}^{-1}$  should have appeared after the adsorption of  $^{18}\text{O}_2$ . However, no such band was detected, which indicates that the development of the component around  $1070\text{ cm}^{-1}$  is due to background affection.

Let us discuss the doublet at  $865$  and  $859\text{ cm}^{-1}$  registered in the background spectrum of the reduced sample (Figure 12, spectrum a). Binet et al. [23], on the basis of  $^{13}\text{C}$ -labeling, have concluded that the band is due to residual carbonates and, as the other carbonate bands, is sensitive to reduction. However, in a recent study, a new assignment to  $\text{Ce}=\text{O}$  modes was proposed [22]. Our results do not support the latter supposition because the bands were not sensitive to exchange with  $^{18}\text{O}$ . Moreover, the relative intensities of the two bands, at  $865$  and  $859\text{ cm}^{-1}$ , could be used as an indicator for the fraction of residual carbonates attached to  $\text{Ce}^{3+}$  sites on reduced samples.

### 2.6. Interaction of Reduced $\text{CeO}_2\text{-NR}$ with $\text{O}_2$ at Variable Temperature

The changes in the spectrum of the reduced  $\text{CeO}_2\text{-NR}$  sample (Figure 13) are generally similar to those already described with the other samples. In this case, however, two peroxide bands ( $889$  and  $831\text{ cm}^{-1}$ ) develop at low temperatures. In the  $\nu(\text{OH})$  region, the band at  $3688\text{ cm}^{-1}$  disappears, and two bands at  $3651$  and  $3628\text{ cm}^{-1}$ , typical of oxidized samples, develop. Based on the band intensities, it was estimated that ca. 40% of the  $\text{Ce}^{3+}$  sites had been oxidized at 100 K. An increase in the temperature up to the ambient provoked the appearance of one more peroxide band at  $840\text{ cm}^{-1}$  (not shown), while the superoxide band totally disappeared. The peroxide species at  $889$  and  $831\text{ cm}^{-1}$  were still observable at 373 K.

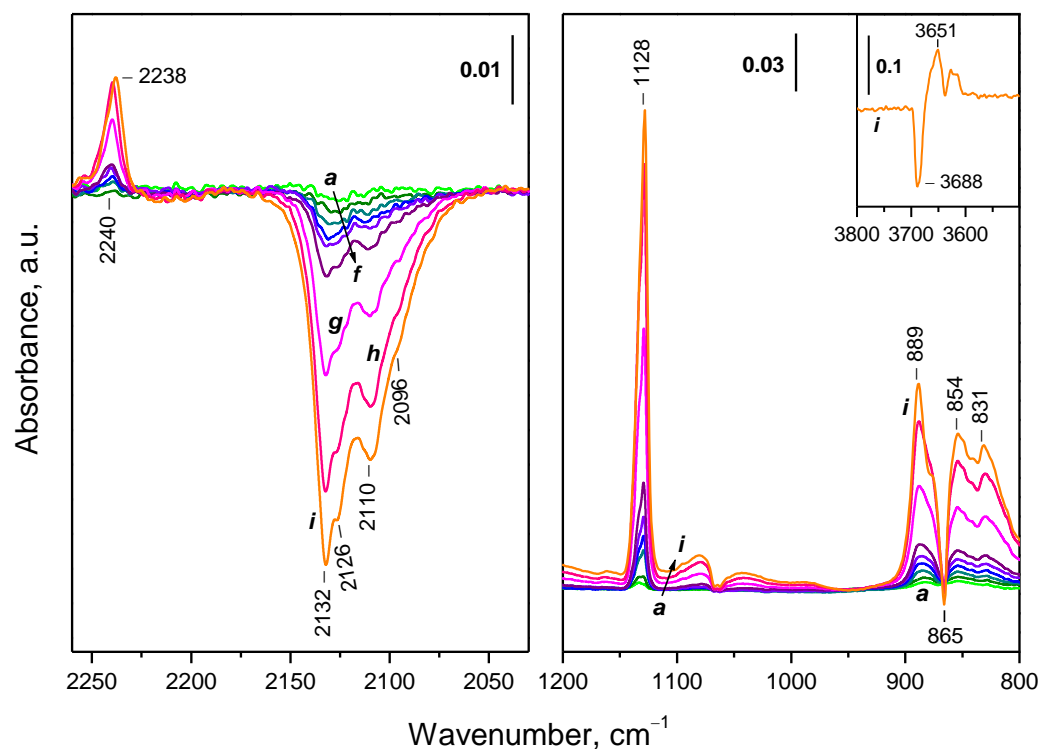


**Figure 13.** Changes in the FTIR spectra of reduced CeO<sub>2</sub>-NR samples after subsequent dosing small amounts of O<sub>2</sub> to the sample at 100 K (a–h) and in the presence of 2 mbar of O<sub>2</sub> (i).

### 2.7. Interaction of the Samples with Oxygen at Ambient Temperature

The studies at ambient temperature allowed us to eliminate the temperature changes of the spectra, which are especially important for the Ce<sup>3+</sup> electronic transition and the OH bands. However, the hydroxyl spectra of the CeO<sub>2</sub>-NP sample were too noisy to allow a precise analysis.

#### 2.7.1. CeO<sub>2</sub>-NC

Small doses of O<sub>2</sub> were successively added to the reduced CeO<sub>2</sub>-NC sample, and after each dose, a spectrum was recorded. Dosage of oxygen leads to erosion of the 2110 cm<sup>-1</sup> band, preferentially from its higher-frequency side (Figure S7, left inset). However, even in the presence of gas-phase oxygen in the cell, the band did not totally disappear, i.e., some Ce<sup>3+</sup> cations (ca. 10%) resisted fast oxidation even at ambient temperature.

The addition of oxygen also provoked the development of an O<sub>2</sub><sup>-</sup> band at 1126 cm<sup>-1</sup> with two satellites at 1112 and 1139 cm<sup>-1</sup> (see the inset in Figure S7). The satellites are attributed to additive and subtractive combination modes of this band. The overtone is also detected at 2236 cm<sup>-1</sup> (Figure S7, main panel). A careful inspection of the spectra also reveals that a very weak peroxide band at 810 cm<sup>-1</sup> developed during oxygen dosage.

In the OH region, the band at 3680 cm<sup>-1</sup> is also gradually eroded and practically disappears in the presence of O<sub>2</sub> in the gas phase (Figure 14, spectrum b). Bands at 3652 and 3631 cm<sup>-1</sup>, typical of freshly activated samples, emerged at its expense (Figure 14, spectrum c). Therefore, we can propose that the O<sub>2</sub><sup>-</sup> species are located at the same sites where the terminal OH groups were originally situated.

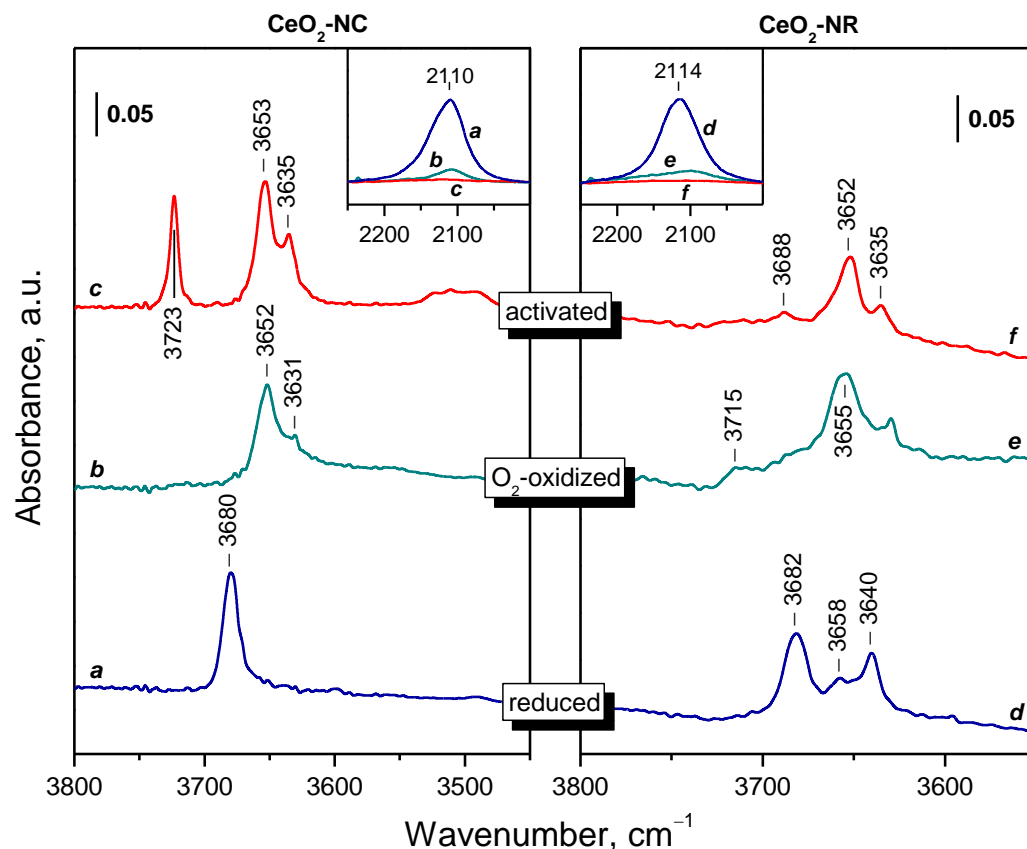


**Figure 14.** FTIR spectra at ambient temperature (hydroxyl stretching region) of CeO<sub>2</sub>-NC (a–c) and CeO<sub>2</sub>-NR (d–f). Samples were reduced with H<sub>2</sub> at 773 K (a,d), re-oxidized by 8 mbar O<sub>2</sub> (b,e), and freshly activated (oxidized) samples (c,f). The insets show the region of the Ce<sup>3+</sup> electronic transition where the spectra are baseline corrected.

Oxygen dosage leads to a gradual shift of the carbonate bands to their original positions with the oxidized sample, and this conversion was full in the presence of gaseous O<sub>2</sub>.

### 2.7.2. CeO<sub>2</sub>-NR

The changes in the spectra registered after dosing oxygen to the reduced CeO<sub>2</sub>-NR sample (See Figure S8) are similar to those already described for CeO<sub>2</sub>-NC. Therefore, here, we will highlight only the main peculiarities.

Here, again, a small fraction of Ce<sup>3+</sup> sites (ca. 13.5%) remained after the interaction of the sample with oxygen at ambient temperature. In the hydroxyl region, oxygen dosage led to gradual conversion to a spectrum typical of the oxidized sample. In this case, however, a small band due to terminal OH species appeared at 3715 cm<sup>-1</sup> (Figure 14, spectrum e). We note that a similar band was detected on the oxidized sample at lower evacuation temperatures. The peroxide species were with negligible concentration. Similar results were obtained with the CeO<sub>2</sub>-NP sample.

## 3. Discussion

### 3.1. Species Formed during Adsorption of O<sub>2</sub> on Oxidized and Reduced Ceria

On oxidized ceria, even after evacuation of the samples at 773 K, we have observed only molecularly adsorbed O<sub>2</sub> by a weak band at 1555–1553 cm<sup>-1</sup>. Although some authors report that no reactive O<sub>2</sub> adsorption occurs on oxidized ceria [19,35], others have observed superoxides with non-reduced samples evacuated at 673 K [32]. In our experiments with oxidized samples, we treated them in O<sub>2</sub> immediately before evacuation at the target temperature (573–773 K). Note that ceria is very easily reduced, and even a minor amount of

organic contaminants originally present in the sample or introduced during the experiments could lead to the production of a small amount of  $\text{Ce}^{3+}$  during the thermal treatment.

As a homonuclear diatomic molecule,  $\text{O}_2$  has no IR active mode. However, after adsorption, the symmetry is reduced, and the O–O stretching modes, although with low intensity, become IR observable. The same phenomenon has been observed for similar molecules, such as  $\text{N}_2$  and  $\text{H}_2$  [49].

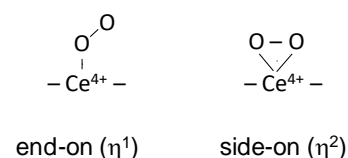
The possible active site on ceria for adsorption of molecular oxygen is coordinatively unsaturated (cus)  $\text{Ce}^{4+}$  cations and hydroxyl groups. The results presented in Figure S5 (spectra a–c) clearly show that the  $\nu(\text{O–O})$  band increases in intensity with sample dehydroxylation, which indicates that the principal adsorption sites are  $\text{Ce}^{4+}$  cations. Indeed,  $\text{Ce}^{4+}$  hydroxyls are of weak acidity, and their complexes with  $\text{O}_2$  are expected to be very weak. The conclusion that OH groups are not active sites for adsorption of molecular  $\text{O}_2$  is consistent with the lack of molecularly adsorbed  $\text{O}_2$  on the hydrated sample (reduced, evacuated at 573 K, and then re-oxidized at 100 K).

The  $\nu(\text{O–O})$  band was observed at  $1553\text{ cm}^{-1}$  with the reduced sample evacuated at 773 K and then oxidized at 100 K (Figure S5, spectrum d). Its intensity was only half of the intensity observed with the oxidized sample evacuated at the same temperature. This suggests that the fast oxidation at 100 K creates some cus  $\text{Ce}^{4+}$  sites acting as adsorption centers.

On reduced ceria, we have detected two more types of adsorbed dioxygen species: superoxide and peroxide. The  $^{18}\text{O}_2$  isotopic experiments confirmed the assignment. This is in general agreement with literature data [17,19,32–35].

Superoxide ion is a monovalent radical produced as a result of one-electron reduction of dioxygen and thus has an O–O bond order of ca. 1.5. Consequently, the  $\nu(\text{O–O})$  stretching frequency is lower as compared to  $\text{O}_2$ . This is consistent with the observation of the superoxide band around  $1130\text{ cm}^{-1}$ . Simple stoichiometric considerations show that two  $\text{O}_2^-$  radicals are necessary to formally substitute one  $\text{O}^{2-}$  anion.

There are two possible configurations of the adsorbed superoxo species: end-on ( $\eta^1$ ) or side-on ( $\eta^2$ ) [50], as shown in Scheme 1:



**Scheme 1.** Possible configurations of superoxo species on ceria.

If the end-on configuration is realized, the  $\text{Ce}^{4+}(\text{}^{16}\text{O}^{18}\text{O})^-$  species should manifest two bands, depending on the position of the labeled atom. In our experiments, we have not detected  $\text{Ce}^{4+}(\text{}^{16}\text{O}^{18}\text{O})^-$  isotopologues. However, Li et al. [34], performing co-adsorption of  $^{16}\text{O}_2$  and  $^{18}\text{O}_2$ , succeeded in detecting  $(\text{}^{16}\text{O}^{18}\text{O})^-$  species and reported they were characterized by one band only at  $1095\text{ cm}^{-1}$ . This indicates a side-on configuration of the superoxo species on ceria.

Consider now the peroxo species. In peroxides, the oxygen atoms are linked by a single covalent bond, and consequently, the  $\nu(\text{O–O})$  modes are observed at lower frequencies as compared to superoxo species. In contrast to superoxide and similarly to  $\text{O}^{2-}$ , it is a divalent anion. This makes peroxide anion suitable to fill oxygen vacancies on ceria.

Pushkarev et al. [35] have reported that peroxides are not formed when ceria is reduced at 573 K but appeared on 673 K reduced samples. Similar conclusions were made by Li et al. [33,34], who did not observe peroxides on ceria reduced by treatment in vacuo at 1000 K but detected them on a hydrogen-reduced sample. This is in agreement with DFT studies [51] indicating that  $\text{O}_2$  interaction with oxygen vacancies on ceria produces peroxides. Thus, it appears that peroxides should acquire a bridging configuration.

Raman studies report two kinds of peroxo species on ceria, characterized by bands at ca.  $860$  and  $830\text{ cm}^{-1}$  [19,35]. A band at  $883\text{ cm}^{-1}$  has been reported in IR studies [21].

Interesting results have been reported by Bashir and Idriss [52]. They adsorbed H<sub>2</sub>O<sub>2</sub> on ceria and detected IR bands at 890, 850, and 835 cm<sup>-1</sup>. The former band was attributed to side-on peroxide, and the other two bands were attributed to bridging species. The band at 890 cm<sup>-1</sup> almost disappeared after the 363 K evacuation, while the other two bands were still observable after the 433 K evacuation. The similarity of these bands to the bands appearing after O<sub>2</sub> adsorption on reduced ceria confirms their assignment to peroxides.

Surprisingly, the formation of Ce<sup>4+</sup>-OOH<sup>-</sup> species has not been reported. In fact, this possibility has been considered but rejected on the basis of the expectation that OOH<sup>-</sup> species should absorb at considerably higher wavenumbers [52]. However, analysis of summarized literature data [50] indicates that OOH<sup>-</sup> species absorb at relatively low frequencies. Thus, it has been reported that Ti-OOH species produced by H<sub>2</sub>O<sub>2</sub> adsorption on Ti silicalite sieve are characterized by a ν(O-O) band at 837 cm<sup>-1</sup> and a broad ν(O-O) band around 3400 cm<sup>-1</sup> [53]. Indeed, H<sub>2</sub>O<sub>2</sub> is a weak acid, and the protons from the OOH<sup>-</sup> groups should tend to form H-bonds. This makes the OH mode of OOH<sup>-</sup> species difficult to distinguish from H-bonded hydroxyls. We note that the OOH<sup>-</sup> moiety is univalent, and, as will be shown below, the formation of Ce-OOH species will answer some open and unresolved questions in ceria surface chemistry.

To form OOH species, a source of hydrogen is necessary. One possible source is the residual OH groups. However, it seems that dissolved hydrogen is a more playable source. A look at Figure 11B shows that peroxide species absorbing in the 850–820 cm<sup>-1</sup> spectral region are readily formed, with samples having a high amount of dissolved hydrogen. Therefore, we propose that these peroxide species are actually hydroperoxides. By analogy, we may suggest that the same accounts for the band at 810 cm<sup>-1</sup>. In contrast, the band at 890 cm<sup>-1</sup> is typical of the hydrogen-free sample, which indicates that it is due to H-free peroxide (O<sub>2</sub><sup>2-</sup>) species.

### 3.2. Ce<sup>3+</sup> Sites Involved in Fast Oxidation

Based on our results, we can divide the Ce<sup>3+</sup> sites on reduced ceria according to their reactivity into three groups:

1. Ce<sup>3+</sup> cations that are fast oxidized at 100 K;
2. Ce<sup>3+</sup> cations fast oxidized between 100 and 293 K, and
3. Ce<sup>3+</sup> cations resist oxidation at 293 K but oxidize at slightly higher temperatures, up to 393 K.

The fraction of the sites in the third group is relatively small, about 10–15%, depending on the pretreatment conditions. This is probably a problem of accessibility because their Ce<sup>3+</sup> electronic transition band is broad, suggesting some heterogeneity. This does not exclude the possibility they are located at subsurface layers.

The fractions of the other two kinds of Ce<sup>3+</sup> sites are abruptly equal. This suggests that they are surface-situated but differ in reactivity.

Consider first the sites fast oxidized at 100 K. It appears that they are of several different kinds, at least sites connected with OH groups, sites connected with residual carbonates, and sites not connected to carbonates or hydroxyls.

Looking at the spectra presented in Figure 7, one could conclude that the Ce<sup>3+</sup> sites attached to OH groups are fast oxidized with simultaneous production of O<sub>2</sub><sup>-</sup> species according to the following hypothetical reaction:



However, a careful analysis of the spectra indicates that the situation is much more complicated. Thus, if Reaction (1) occurred, the OH band should undergo an additional shift at full oxidation (including the two Ce<sup>3+</sup> sites), which was not observed in the experiments.

Note that during the fast oxidation of Ce<sup>3+</sup> sites, the formation of superoxides and peroxides, as well as the concomitant changes (e.g., in the hydroxyl or carbonate regions), proceed in parallel. We attribute this to the so-called “wall effect”. Reactive adsorption of

oxygen is irreversible, and O<sub>2</sub> molecules interact with the first appropriate site they meet along the way. Thus, the ratio between the different Ce<sup>3+</sup> sites oxidized at 100 K will not be determined by the differences in their affinity for oxygen. From this, we may conclude that all Ce<sup>3+</sup> sites participating in the fast oxidation are accessible and situated on the surface.

Consequently, an important conclusion on the location of surface carbonates can be made. There are some arguments that they are situated not on the subsurface [25,27]. However, it appears that on reduced samples, at least part of them are connected to surface Ce<sup>3+</sup> sites. This could happen if the carbonates are located on the surface or in the subsurface layer.

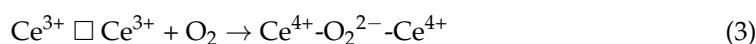
Bridging hydroxyls on ceria are of II or III type, i.e., connected with two or three cerium cations. However, it is important to note that for samples evacuated at 773 K, the regular crystal planes are dehydroxylated, and the residual hydroxyls are located at edges, corners, or other defect sites. Therefore, the Ce<sup>3+</sup> ions connected to OH groups should be highly accessible.

A widely accepted reaction of ceria reduction is that leading to the formation of oxygen vacancies:

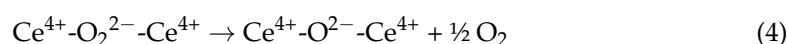


where  $\square$  denotes an oxygen vacancy.

Reoxidation needs the formation of a divalent anion, and this can be easily achieved according to the reaction:

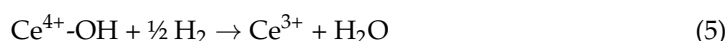


At temperatures above ca. 473 K, peroxides completely decompose, and the original state typical of oxidized ceria surface is restored:



The most probably analogous reaction occurs when Ce<sup>3+</sup> sites from bridging hydroxyls are oxidized because it was already noted that no step oxidation of the two Ce<sup>3+</sup> sites was detected.

It was noted that the formation of superoxide species cannot be explained by the model of surface oxygen vacancy and is rather indicative of the presence of low-coordinated Ce<sup>3+</sup> sites [51]. We propose that such Ce<sup>3+</sup> sites can be produced by reduction of Ce<sup>4+</sup> sites connected to terminal OH groups:



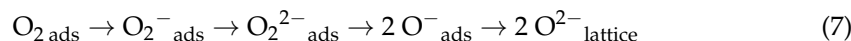
Indeed, the results presented in Figure 6, Figure 7, and Figure 13 show that after the fast oxidation, the terminal OH groups on the CeO<sub>2</sub>-NC sample are not regenerated. It is logical to expect that the charge balance is achieved by the formation of a Ce<sup>4+</sup>-O<sub>2</sub><sup>-</sup> complex, e.g., according to the following reaction:



Thus, one of the possible locations of the Ce<sup>4+</sup>-O<sub>2</sub><sup>-</sup> species is in the place of the original terminal Ce<sup>4+</sup>-OH groups.

It was established that oxidation at 100 K leads to obtaining a highly stable semi-oxidized state of ceria. A large part of Ce<sup>3+</sup> sites is additionally oxidized between 100 and 293 K. First, some extra superoxide species were produced in this way. This indicates the proceeding of reaction (6) and evidences the existence of a fraction of less reactive isolated Ce<sup>3+</sup> sites. However, the superoxide band started to decline with the rise in temperature, and particular peroxide species were produced at its expense.

Based on similar observations, Li et al. [33] proposed the following evolution of the oxygen adspecies on ceria:



According to our results, these consecutive conversions could be divided into two independent pathways: evolution of peroxo and evolution of superoxo species.

It was already noted that peroxides could be directly decomposed, thus producing lattice oxygen in the place of the oxygen vacancy.

Consider now the superoxide species. The fact that they form on isolated ex-Ce<sup>3+</sup> sites indicates that they must evolve by forming monovalent anions. A hypothetical candidate for this is the O<sup>-</sup> anion. However, we have no indication of its formation. In contrast, we already proposed that the bands below 850 cm<sup>-1</sup> characterize hydroperoxo species. Thus, a possible reduction of the Ce<sup>4+</sup>-O<sub>2</sub><sup>-</sup> species is according to the following reaction:



In this case, the interaction proceeds with hydrogen dissolved in ceria. Indeed, it was established that it promotes the formation of hydroperoxides. However, we cannot exclude the possibility of some hydroperoxides being formed with the participation of hydrogen from surface OH groups.

After the decomposition of the Ce<sup>4+</sup>-OOH groups, the original terminal hydroxyls typical of oxidized surface are restored:



The initial stage of this reaction was documented in our IR results (see Figure 6B, spectrum k).

The O<sup>-</sup> radicals are invisible in IR but have been observed on some oxides by ESR [54]. Although suggested [33], these species have not been reported for pure ceria. In any case, we cannot totally rule out the possibility that, under hydrogen-deficient conditions, direct decomposition of O<sub>2</sub><sup>-</sup> to O<sup>-</sup> occurs, the latter ensuring the charge balance instead of OH<sup>-</sup> or OOH<sup>-</sup>.

In conclusion, the evolution of the adsorbed oxygen species on isolated Ce<sup>3+</sup> sites and on oxygen vacancies follows two different and independent routes.

### 3.3. Fine Structure of Ce<sup>3+</sup> Band

In this study, we report for the first time a fine structure of the Ce<sup>3+</sup> electronic band. This can explain the different values of the band position reported in the literature. This work is the first attempt to assign the different components of the band. We realize that additional work has to be performed for the precise attribution, but our results allow us to make some definite conclusions.

At first, it was unambiguously established that the position of the sub-bands strongly depends on the presence of OH group(s) in the first coordination sphere of Ce<sup>3+</sup> cations. Comparison between the spectra of reduced sample evacuated at 773 K and 573 K (Figure 11A, spectra c, and d, respectively) clearly shows that the components around 2133 and 2096–2095 cm<sup>-1</sup> consumed during the fast oxidation at 100 K are much more intense with the highly dehydroxylated sample and therefore should be associated with Ce<sup>3+</sup> sites having no OH groups in the vicinity. The same seems to be also valid for the component at 2105 cm<sup>-1</sup>. In contrast, the component at 2109 cm<sup>-1</sup> appears with enhanced intensity with the hydroxylated sample and thus can be associated with Ce<sup>3+</sup> cations connected with the extra OH groups on this sample (3664 cm<sup>-1</sup>).

On the basis of the above considerations, one could expect that Ce<sup>3+</sup> cations bound on residual carbonates should also possess a specific spectral behavior. Unfortunately, on the basis of our experiments, we are not able to draw any definite conclusions at this stage.

Comparison between the samples reduced at different temperatures (Figure 11A, spectra a–c) clearly shows that the component at  $2126\text{ cm}^{-1}$  corresponds to  $\text{Ce}^{3+}$  sites that are produced more difficult during reduction.

The sites that resist fast oxidation at 100 K but are oxidized at higher temperatures up to 293 K give rise to a broad  $\text{Ce}^{3+}$  band with two resolved components at 2118 and  $2112\text{ cm}^{-1}$ .

Finally, the small fraction of sites residual to oxidation at 293 K produces a broad band at  $2109\text{ cm}^{-1}$ . Since the band does not differ significantly from the above-discussed band, we could suggest that the inertness of these sites could be due to low accessibility. It is not excluded as they are in the subsurface layer.

At the beginning of this study, we aimed to establish a clear relationship between the band components and the exposed crystal facets. However, it appears that the positions of the components depend on too many factors, and at this stage, we desist from making definite conclusions. Further specially designed experiments are necessary to answer this question and to establish eventual dependence between the component position and location of the  $\text{Ce}^{3+}$  on different crystal planes and edges.

### 3.4. Oxidation of Sorbed $\text{H}_2$

It was reported that hydrogen is stored on ceria below 773 K and released above this temperature [16,55]. A surprising observation in this study is the ability of  $\text{O}_2$  to oxidize dissolved hydrogen at 100 K in the absence of any noble metal. Although the fraction of this hydrogen is relatively small, the phenomenon could be of great importance for catalysis because it demonstrates the high reactivity of hydrogen in ceria. We also found that this hydrogen strongly affects the conversion pathway of superoxide species. Since it is invisible in IR, we suggest that some of the results reported in the literature have been affected by dissolved hydrogen. Our results indicate that hydrogen is more stable on partly reduced samples, and thus, it can be present in some amount even after evacuation at  $T > 773\text{ K}$ . Therefore, dissolved hydrogen could exist during the proceeding of some catalytic redox reactions even at temperatures higher than 773 K.

The nature of hydrogen dissolved in ceria is still not well known. It has recently been pointed out that the question of whether H atoms enter the bulk or are chemisorbed on the surfaces of  $\text{CeO}_2$  is a subject of debate [56]. Our results rather support the view that at least part of this hydrogen is in the bulk and needs to migrate to the surface in order to be oxidized. Indeed, the major part of the dissolved hydrogen is oxidized at temperatures up to ambient one.

## 4. Materials and Methods

### 4.1. Synthesis of the Samples

A hydrothermal method was used for the synthesis of nanosized samples of  $\text{CeO}_2$  with different morphologies (cubes, rods, and polyhedra) [57,58]. 85 mL aqueous solution of 5 g  $\text{Ce}(\text{NO}_3)_3 \cdot 6\text{H}_2\text{O}$  (Fluka, Buchs, Switzerland, 99% purity) was added with vigorous stirring to 150 mL alkaline solution of 54 g NaOH (Merck, Darmstadt, Germany, 99% purity) in water. After obtaining a suspension, stirring was continued for another 30 min, after which the reaction mixture was transferred to an autoclave. Nanocubes (sample  $\text{CeO}_2\text{-NC}$ ) and nanorods (sample  $\text{CeO}_2\text{-NR}$ ) were obtained after “aging” in an autoclave for 24 h at 453 and 373 K, respectively. The conditions for the synthesis of the nanopolyhedra (sample  $\text{CeO}_2\text{-NP}$ ) are identical to those of the nanorods, but the alkaline solution used was more diluted (9 g NaOH in 150 mL water). Finally, the suspensions were centrifuged, and the precipitates were washed with deionized water, dried at 393 K, and calcined at 673 K for 2 h.

### 4.2. Gases

All non-labeled gases used for the IR and TPR experiments were provided by Messer (Bad Soden, Germany): hydrogen (>99.999%); helium (99.999%); oxygen (99.999%), 5%  $\text{O}_2/\text{He}$  ( $\text{O}_2$  99.95%) and 10%  $\text{H}_2/\text{Ar}$  ( $\text{H}_2$  99.95%). Labeled oxygen,  $^{18}\text{O}_2$ , was provided by ISOTECH (Miami, OH, USA) and had an isotopic purity of 99 atom %  $^{18}\text{O}$ .

### 4.3. Methods

#### 4.3.1. FTIR Spectroscopy

FTIR spectra were registered with a Thermo Scientific Nicolet 6700 FTIR Spectrometer equipped (Madison, WI, USA) with an MCT/A detector. The spectral resolution was  $2\text{ cm}^{-1}$ , and 64 scans were accumulated for each spectrum. Self-supporting wafers (ca.  $15\text{ mg cm}^{-2}$ ) were prepared from the sample powders and treated directly in a purpose-made IR cell connected to a vacuum-adsorption apparatus with a residual pressure below  $10^{-4}\text{ Pa}$ . Before the experiments, the samples were activated by heating them in oxygen (100 mbar) for 30 min at 773 K, followed by 30 min of evacuation at the same temperature.

To obtain an oxidized sample, the pellet was treated at the desired activation temperature for 10 min in the presence of 2 mbar of  $\text{O}_2$  and then evacuated for 30 min at the same temperature.

To obtain reduced samples, the pellets were treated in 100 mbar of  $\text{H}_2$  for 1 h at 773 K, followed by 1 h evacuation at the desired temperature, typically at 773 K. In this way, all eventually stored hydrogen (characterized by a TPD peak at 580 K [43]) was removed. When lower evacuation temperatures were applied, this was specially noted.

For all low-temperature measurements, the IR cell was initially cooled using liquid nitrogen, and then 2 mbar of He was added to the system in order to improve heat transfer.

Low-temperature adsorption of  $\text{O}_2$  on reduced samples was performed either by successive addition of small doses of  $\text{O}_2$  or by direct introduction of oxygen at 2 mbar pressure. Then, the sample temperature was gradually raised. Interaction with  $\text{O}_2$  at 313–400 K was studied by heating the sample at the target temperature, followed by cooling to ambient temperature.

For the experiments performed at ambient temperature, small doses of  $\text{O}_2$  were successively added to the system.

#### 4.3.2. Temperature-Programmed Reduction

Temperature-programmed reduction with hydrogen ( $\text{H}_2$ -TPR) was carried out using a ChemBET TPR/TPD apparatus (Quantachrome Instruments, Boynton Beach, FL, USA) equipped with a thermal conductivity detector. A nitrogen/ethanol cold trap (placed before the detector) was used to eliminate water vapor from the gas flow. Before the TPR, the samples were heated to 773 K in a flowing stream of 5%  $\text{O}_2/\text{He}$ . TPR curves were recorded while reducing the samples ( $\sim 40\text{ mg}$ ) in a 10%  $\text{H}_2/\text{Ar}$  mixture at a flow rate of  $20\text{ mL min}^{-1}$  and increasing the temperature from room temperature to 1273 K at a ramp rate of  $10\text{ K min}^{-1}$ .

#### 4.3.3. Transmission Electron Microscopy

The Transmission Electron Microscopy (TEM) study was performed with a JEOL 2100 transmission electron microscope (TEM, Tokyo, Japan) at an accelerating voltage of 200 kV equipped with X-ray energy-dispersive spectrometer (XEDS) Oxford Instruments (Abingdon, UK), X-MAX N 80 T; CCD Camera ORIUS 1000, 11 Mp, GATAN (Pleasanton, CA, USA). Before examination, each sample was suspended in ethanol solution and dripped onto a standard holey carbon/Cu grid. The data analysis was carried out using the Digital Micrograph™ software (version 3.7.4) from Gatan.

#### 4.3.4. X-ray Diffraction

Powder X-ray diffraction (XRD) analysis was performed with a Bruker D8 Advance diffractometer with CuK $\alpha$  radiation and a LynxEye solid position-sensitive detector (Bruker AXS, Karlsruhe, Germany). XRD patterns were recorded in the range of  $5.3$  to  $80^\circ 2\theta$  with a constant step of  $0.02^\circ 2\theta$  and a counting time of 17.5 s per step. The mean crystallite size was calculated according to Scherrer's equation with Topas v.4.2 software (Bruker AXS, Karlsruhe, Germany).

#### 4.3.5. BET Surface Area

Brunauer-Emmett-Teller (BET) surface areas were determined using low-temperature (77.4 K) nitrogen adsorption in a NOVA 1200e apparatus (Quantachrome Instruments, Boynton Beach, FL, USA). The samples were degassed overnight at 473 K under vacuum to ensure a clean, dry surface.

### 5. Conclusions

- No autoreduction in  $\text{Ce}^{4+}$  to  $\text{Ce}^{3+}$  occurs during the evacuation of pure ceria nanoparticles at 573–773 K.
- Reduction in ceria with  $\text{H}_2$  at 773 K leads to the formation of  $\text{Ce}^{3+}$  cations on the surface, which are monitored in the IR spectra by a band at 2133–2094  $\text{cm}^{-1}$ . This band possesses a fine structure, well resolved at 100 K. The positions of the individual components depend on the environment of  $\text{Ce}^{3+}$ , including the presence of nearby OH groups and likely residual carbonates.
- Even at 100 K, part of the  $\text{Ce}^{3+}$  sites on reduced ceria are quickly oxidized by  $\text{O}_2$ . These sites are situated on the surface and include all  $\text{Ce}^{3+}$  cations bound to OH groups and carbonates.
- Depending on the location of the  $\text{Ce}^{3+}$  sites,  $\text{O}_2^-$  or  $\text{O}_2^{2-}$  are produced during the fast oxidation of reduced ceria at 100 K.
- Some  $\text{Ce}^{3+}$  sites resist oxidation at 100 K but are oxidized at higher temperatures, between 100–400 K. These sites are also assumed to be surface situated, but a location in subsurface layers is not excluded.
- Peroxide ( $\text{O}_2^{2-}$ ) species decompose to give lattice oxygen, while superoxides first convert to hydroperoxides ( $\text{OOH}^-$ ) and then to terminal OH groups.
- $\text{H}_2$  dissolves in reduced ceria and is not completely removed upon evacuation at temperatures <773 K. Part of this hydrogen is also fast oxidized at 100 K, which demonstrates its high reactivity.

**Supplementary Materials:** The following supporting information can be downloaded at: <https://www.mdpi.com/article/10.3390/catal14010045/s1>: Figure S1: Background spectra of the  $\text{CeO}_2$ -NR sample; Figure S2: Background spectra of the  $\text{CeO}_2$ -NP sample; Figure S3: Spectra of the  $\text{Ce}^{3+}$  electronic band in presence of  $\text{CO}_2$  and  $\text{H}_2\text{O}$ ; Figure S4: Temperature effect on the spectra in the hydroxyl and carbonate regions; Figure S5: IR spectra of molecularly adsorbed  $\text{O}_2$ ; Figure S6: Effect of oxidation of  $\text{CeO}_2$ -NC on the position of the carbonate bands; Figure S7: IR spectra of oxygen adsorbed on  $\text{CeO}_2$ -NC at ambient temperature; Figure S8: IR spectra of oxygen adsorbed on  $\text{CeO}_2$ -NR at ambient temperature; Table S1: Consumption of  $\text{H}_2$  during TPR of the samples.

**Author Contributions:** Conceptualization, M.M. and K.H.; methodology, K.H.; investigation, K.C. and N.D.; writing—original draft preparation, K.H.; writing—review and editing, K.C., N.D., M.M. and K.H.; visualization, K.C. and K.H.; funding acquisition, M.M. and K.H. All authors have read and agreed to the published version of the manuscript.

**Funding:** This research was funded by the Bulgarian Science Fund, grant number KII-06-H-59/5/2021.

**Data Availability Statement:** The data presented in this study are available in the article and the Supplementary Material.

**Acknowledgments:** Research equipment of the National Centre for Mechatronics and Clean Technologies was used for the experiments (project BG05M2OP001-1.001-0008, funded by the European Regional Development Fund under the Operational Program “Science and Education for Smart Growth 2014–2020”). Thanks are also due to: D. Kovacheva for XRD analysis, L. Mihaylov for TEM analysis, and L. Dimitrov for sample synthesis.

**Conflicts of Interest:** The authors declare no conflicts of interest.

### References

1. Trovarelli, A.; de Leitenburg, C.; Boaro, M.; Dolcetti, G. The utilization of ceria in industrial catalysis. *Catal. Today* **1999**, *50*, 353–367. [[CrossRef](#)]

2. Chung, C.-H.; Tu, F.-Y.; Chiu, T.-A.; Wu, T.-T.; Yu, W.-Y. Critical roles of surface oxygen vacancy in heterogeneous catalysis over ceria-based materials: A selected review. *Chem. Lett.* **2021**, *50*, 856–865. [[CrossRef](#)]
3. Chuen, W.C.; Haile, S.M. A thermochemical study of ceria: Exploiting an old material for new modes of energy conversion and CO<sub>2</sub> mitigation. *Phil. Trans. R. Soc. A* **2010**, *368*, 3269–3294.
4. Ganduglia-Pirovano, M.V.; Hofmann, A.; Sauer, J. Oxygen vacancies in transition metal and rare earth oxides: Current state of understanding and remaining challenges. *Surf. Sci. Rep.* **2007**, *62*, 219–270. [[CrossRef](#)]
5. Rozhin, P.; Melchionna, M.; Fornasiero, P.; Marchesan, S. Nanostructured ceria: Biomolecular templates and (bio)applications. *Nanomaterials* **2021**, *11*, 2259. [[CrossRef](#)]
6. Song, G.; Cheng, N.; Zhang, J.; Huang, H.; Yuan, Y.; He, X.; Luo, Y.; Huang, K. Nanoscale cerium oxide: Synthesis, biocatalytic mechanism, and applications. *Catalysts* **2021**, *11*, 1123. [[CrossRef](#)]
7. Putna, E.S.; Vohs, J.M.; Gorte, R.J. Evidence for weakly bound oxygen on ceria films. *J. Phys. Chem.* **1996**, *100*, 17862–17865. [[CrossRef](#)]
8. Yao, H.C.; Yao, Y.F.Y. Ceria in automotive exhaust catalysts. I. Oxygen storage. *J. Catal.* **1984**, *86*, 254–265. [[CrossRef](#)]
9. Laachir, A.; Perrichon, V.; Badri, A.; Lamotte, J.; Catherine, E.; Lavalley, J.C.; El Fallah, J.; Hilaire, L.; Le Normand, F.; Quéméré, E.; et al. Reduction of CeO<sub>2</sub> by hydrogen. Magnetic susceptibility and Fourier-transform infrared, ultraviolet and X-ray photoelectron spectroscopy measurements. *J. Chem. Soc. Faraday Trans.* **1991**, *87*, 1601–1609. [[CrossRef](#)]
10. Holgado, J.P.; Munuera, G. XPS/TPR study of the reducibility of M/CeO<sub>2</sub> catalysts (M = Pt, Rh): Does junction effect theory apply? In *Studies in Surface Science and Catalysis*; Frennet, A., Bastin, J.M., Eds.; Elsevier: Amsterdam, The Netherlands, 1995; Volume 96, pp. 109–122.
11. Rao, G.R. Influence of metal particles on the reduction properties of ceria-based materials studied by TPR. *Bull. Mater. Sci.* **1999**, *22*, 89–94. [[CrossRef](#)]
12. Giordano, F.; Trovarelli, A.; Leitenburg, C.; Giona, M. A model for the temperature-programmed reduction of low and high surface area ceria. *J. Catal.* **2000**, *193*, 273–282. [[CrossRef](#)]
13. Fally, F.; Perrichon, V.; Vidal, H.; Kaspar, J.; Blanco, G.; Pintado, J.M.; Bernal, S.; Colon, G.; Daturi, M.; Lavalley, J.C. Modification of the oxygen storage capacity of CeO<sub>2</sub>–ZrO<sub>2</sub> mixed oxides after redox cycling aging. *Catal. Today* **2000**, *59*, 373–386. [[CrossRef](#)]
14. Ayastuy, J.L.; Gil-Rodríguez, A.; González-Marcos, M.P.; Gutiérrez-Ortiz, M.A. Effect of process variables on Pt/CeO<sub>2</sub> catalyst behaviour for the PROX reaction. *Int. J. Hydrogen Energy* **2006**, *31*, 2231–2242. [[CrossRef](#)]
15. Lee, J.; Ryou, Y.S.; Chan, X.; Kim, T.J.; Kim, D.H. How Pt interacts with CeO<sub>2</sub> under the reducing and oxidizing environments at elevated temperature? The origin of improved thermal stability of Pt/CeO<sub>2</sub> compared to CeO<sub>2</sub>. *J. Phys. Chem C* **2016**, *120*, 25870–25879. [[CrossRef](#)]
16. Agarwal, S.; Mojet, L.L.; Lefferts, L.; Datye, A.K. Ceria nanoshapes-structural and catalytic properties. In *Catalysis by Materials with Well-Defined Structures*; Elsevier: Amsterdam, The Netherlands, 2015; pp. 31–70.
17. Qiao, Z.-A.; Wu, Z.; Dai, S. Shape-controlled ceria-based nanostructures for catalysis applications. *ChemSusChem* **2013**, *6*, 1821–1833. [[CrossRef](#)]
18. Sun, C.; Li, H.; Chen, L. Nanostructured ceria-based materials: Synthesis, properties, and applications. *Energy Environ. Sci.* **2012**, *5*, 8475–8505. [[CrossRef](#)]
19. Wu, Z.; Li, M.; Howe, J.; Meyer, H.M.; Overbury, S.H. Probing defect sites on CeO<sub>2</sub> nanocrystals with well-defined surface planes by Raman spectroscopy and O<sub>2</sub> adsorption. *Langmuir* **2010**, *26*, 16595–16606. [[CrossRef](#)]
20. Wu, W.; Savereide, L.M.; Notestein, J.; Weitz, E. In-situ IR spectroscopy as a probe of oxidation/reduction of Ce in nanostructured CeO<sub>2</sub>. *Appl. Surf. Sci.* **2018**, *445*, 548–554. [[CrossRef](#)]
21. Zotin, F.M.Z.; Tournayan, L.; Varloud, J.; Perrichon, V.; Frety, R. Temperature-programmed reduction: Limitation of the technique for determining the extent of reduction of either pure ceria or ceria modified by additives. *Appl. Catal. A* **1993**, *98*, 99–114. [[CrossRef](#)]
22. Afrin, S.; Bollini, P. On the utility of Ce<sup>3+</sup> spin-orbit transitions in the interpretation of rate data in ceria catalysis: Theory, validation, and application. *J. Phys. Chem. C* **2023**, *127*, 234–247. [[CrossRef](#)]
23. Binet, C.; Badri, A.; Lavalley, J.-C. A spectroscopic characterization of the reduction of ceria from electronic transitions of intrinsic point defects. *J. Phys. Chem.* **1994**, *98*, 6392–6398. [[CrossRef](#)]
24. Binet, C.; Daturi, M.; Lavalley, J.-C. IR study of polycrystalline ceria properties in oxidised and reduced states. *Catal. Today* **1999**, *50*, 207–225. [[CrossRef](#)]
25. Mihaylov, M.Y.; Ivanova, E.Z.; Aleksandrov, H.A.; Petkov, P.S.; Vayssilov, G.N.; Hadjiivanov, K.I. FTIR and density functional study of NO interaction with reduced ceria: Identification of N<sub>3</sub><sup>-</sup> and NO<sup>2-</sup> as new intermediates in NO conversion. *Appl. Catal. B* **2015**, *176–177*, 107–119. [[CrossRef](#)]
26. Mihaylov, M.Y.; Ivanova, E.Z.; Aleksandrov, H.A.; Petkov, P.S.; Vayssilov, G.N.; Hadjiivanov, K.I. Formation of N<sub>3</sub><sup>-</sup> during interaction of NO with reduced ceria. *Chem. Commun.* **2015**, *51*, 5668–5671. [[CrossRef](#)]
27. Mihaylov, M.Y.; Ivanova, E.Z.; Vayssilov, G.N.; Hadjiivanov, K.I. Revisiting ceria-NO<sub>x</sub> interaction: FTIR studies. *Catal. Today* **2020**, *357*, 613–620. [[CrossRef](#)]
28. Li, H.; Zhang, P.; Li, G.; Lu, J.; Wu, Q.; Gu, Y. Stress measurement for nonstoichiometric ceria films based on Raman spectroscopy. *J. Alloys Compd.* **2016**, *682*, 132–137. [[CrossRef](#)]

29. Bozon-Verduraz, F.; Bensalem, A. IR studies of cerium dioxide: Influence of impurities and defects. *J. Chem. Soc. Faraday Trans.* **1994**, *90*, 653–657. [[CrossRef](#)]
30. Chen, L.; Fleming, P.; Morris, V.; Holmes, J.D.; Morris, M.A. Size-related lattice parameter changes and surface defects in ceria nanocrystals. *J. Phys. Chem. C* **2010**, *114*, 12909–12919. [[CrossRef](#)]
31. Zhang, B.; Zhang, S.; Liu, B. Effect of oxygen vacancies on ceria catalyst for selective catalytic reduction of NO with NH<sub>3</sub>. *Appl. Surf. Sci.* **2020**, *529*, 147068. [[CrossRef](#)]
32. Descorme, C.; Madier, Y.; Duprez, D. Infrared study of oxygen adsorption and activation on cerium–zirconium mixed oxides. *J. Catal.* **2000**, *196*, 167–173. [[CrossRef](#)]
33. Li, C.; Domen, K.; Maruya, K.; Onishi, T. Dioxygen adsorption on well-outgassed and partially reduced cerium oxide studied by FT-IR. *J. Am. Chem. Soc.* **1989**, *111*, 7683–7687. [[CrossRef](#)]
34. Li, C.; Domen, K.; Maruya, K.-I.; Onishi, T. Oxygen exchange reactions over cerium oxide: An FT-IR study. *J. Catal.* **1990**, *123*, 436–442. [[CrossRef](#)]
35. Pushkarev, V.V.; Kovalchuk, V.I.; d'Itri, J.L. Probing defect sites on the CeO<sub>2</sub> surface with dioxygen. *J. Phys. Chem. B* **2004**, *108*, 5341–5348. [[CrossRef](#)]
36. Cardenas, L.; Molinet-Chinaglia, C.; Loridant, S. Unraveling Ce<sup>3+</sup> detection at the surface of ceria nanopowders by UPS analysis. *Phys. Chem. Chem. Phys.* **2022**, *24*, 22815–22822. [[CrossRef](#)] [[PubMed](#)]
37. Morgan, D.J. Photoelectron spectroscopy of ceria: Reduction, quantification and the myth of the vacancy peak in XPS analysis. *Surf. Interface Anal.* **2023**, *55*, 845–850. [[CrossRef](#)]
38. Xu, Y.; Wang, F.; Liu, X.; Liu, Y.; Luo, M.; Teng, B.; Fan, M.; Liu, X. Resolving a decade-long question of oxygen defects in Raman spectra of ceria-based catalysts at atomic level. *J. Phys. Chem. C* **2019**, *123*, 18889–18894. [[CrossRef](#)]
39. Filtschew, A.; Hofmann, K.; Hess, C. Ceria and its defect structure: New insights from a combined spectroscopic approach. *J. Phys. Chem. C* **2016**, *120*, 6694–6703. [[CrossRef](#)]
40. Schmitt, R.; Nanning, A.; Kraynis, O.; Korobko, R.; Frenkel, A.I.; Lubomirsky, I.; Haile, S.M.; Rupp, J.L.M. A review of defect structure and chemistry in ceria and its solid solutions. *Chem. Soc. Rev.* **2020**, *49*, 554–592. [[CrossRef](#)]
41. Wang, X.; Li, M.; Wu, Z. In situ spectroscopic insights into the redox and acid-base properties of ceria catalysts. *Chin. J. Catal.* **2021**, *42*, 2122–2140. [[CrossRef](#)]
42. Loridant, S. Raman spectroscopy as a powerful tool to characterize ceria-based catalysts. *Catal. Today* **2021**, *373*, 98–111. [[CrossRef](#)]
43. Bruce, L.A.; Hoang, M.; Hughes, A.E.; Turney, T.W. Surface area control during the synthesis and reduction of high area ceria catalyst supports. *Appl. Catal. A* **1996**, *134*, 351–362. [[CrossRef](#)]
44. Badri, A.; Binet, C.; Lavalley, J.-C. An FTIR study of surface ceria hydroxy groups during a redox process with H<sub>2</sub>. *J. Chem. Soc. Faraday Trans.* **1996**, *92*, 4669–4673. [[CrossRef](#)]
45. Tsyganenko, A.A.; Filimonov, V.N. Infrared spectra of surface hydroxyl groups and crystalline structure of oxides. *J. Mol. Struct.* **1973**, *19*, 579–589. [[CrossRef](#)]
46. Vayssilov, G.N.; Mihaylov, M.; Petkov, P.S.; Hadjiivanov, K.I.; Neyman, K.M. Reassignment of the vibrational spectra of carbonates, formates, and related surface species on ceria: A combined density functional and infrared spectroscopy investigation. *J. Phys. Chem. C* **2011**, *115*, 23435–23454. [[CrossRef](#)]
47. Hadjiivanov, K. Identification and characterization of surface hydroxyl groups by infrared spectroscopy. *Adv. Catal.* **2014**, *47*, 99–318.
48. Otsuka, K.; Hatano, M.; Morikawa, A. Hydrogen from water by reduced cerium oxide. *J. Catal.* **1983**, *79*, 493–496. [[CrossRef](#)]
49. Zecchina, A.; Otero Areán, C. Diatomic molecular probes for mid-IR studies of zeolites. *Chem. Soc. Rev.* **1996**, *25*, 187–197. [[CrossRef](#)]
50. Nakamoto, K. *Infrared and Raman Spectra of Inorganic and Coordination Compounds, Part B*, 6th ed.; John Wiley & Sons: Hoboken, NJ, USA, 2009.
51. Preda, G.; Migani, A.; Neyman, K.M.; Bromley, S.T.; Illas, F.; Pacchioni, G. Formation of superoxide anions on ceria nanoparticles by interaction of molecular oxygen with Ce<sup>3+</sup> sites. *J. Phys. Chem. C* **2011**, *115*, 5817–5822. [[CrossRef](#)]
52. Bashir, S.M.; Idriss, H. The reaction of propylene to propylene-oxide on CeO<sub>2</sub>: An FTIR spectroscopy and temperature programmed desorption study. *J. Chem. Phys.* **2020**, *152*, 044712. [[CrossRef](#)]
53. Lin, W.Y.; Frei, H. Photochemical and FT-IR probing of the active site of hydrogen peroxide in Ti silicalite sieve. *J. Am. Chem. Soc.* **2002**, *124*, 9292–9298. [[CrossRef](#)]
54. Anpo, M.; Costentin, G.; Giamello, E.; Lauron-Pernot, H.; Sojka, J. Characterisation and reactivity of oxygen species at the surface of metal oxides. *J. Catal.* **2021**, *393*, 259–280. [[CrossRef](#)]
55. Bernal, S.; Calvino, J.J.; Cifredo, G.A.; Gatica, J.M.; Perez Omil, H.; Pintado, J.M. Hydrogen chemisorption on ceria: Influence of the oxide surface area and degree of reduction. *J. Chem. Soc. Faraday Trans.* **1993**, *89*, 3499–3505. [[CrossRef](#)]
56. Kammert, J.; Moon, J.; Wu, Z. A review of the interactions between ceria and H<sub>2</sub> and the applications to selective hydrogenation of alkynes. *Chin. J. Catal.* **2020**, *41*, 901–914. [[CrossRef](#)]

57. Zabilskiy, M.; Djinović, P.; Tchernychova, E.; Tkachenko, O.P.; Kustov, L.M.; Pintar, A. Nanoshaped CuO/CeO<sub>2</sub> materials: Effect of the exposed ceria surfaces on catalytic activity in N<sub>2</sub>O decomposition reaction. *ACS Catal.* **2015**, *5*, 5357–5365. [[CrossRef](#)]
58. Mai, H.-X.; Sun, L.-D.; Zhang, Y.-W.; Si, R.; Feng, W.; Zhang, H.-P.; Liu, H.-C.; Yan, C.-H. Shape-selective synthesis and oxygen storage behavior of ceria nanopolyhedra, nanorods, and nanocubes. *J. Phys. Chem. B* **2005**, *109*, 24380–24385. [[CrossRef](#)]

**Disclaimer/Publisher’s Note:** The statements, opinions and data contained in all publications are solely those of the individual author(s) and contributor(s) and not of MDPI and/or the editor(s). MDPI and/or the editor(s) disclaim responsibility for any injury to people or property resulting from any ideas, methods, instructions or products referred to in the content.